JOURNAL OF GEOPHYSICAL RESEARCH, VOL. 96, NO. B7, PAGES 12,099–12,125, JULY 10, 1991

Lg and *Rg* Waves on the California Regional Networks From the December 23, 1985 Nahanni Earthquake

LISA A. WALD AND THOMAS H. HEATON

U. S. Geological Survey, Pasadena, California

We investigate *Lg* and *Rg* propagation in California using the central and southern California regional networks. Approximately 550 stations constitute these two short-period networks providing a dense coverage of almost the entire state. The waveforms recorded from the December 23, 1985, Nahanni, Canada, earthquake are used to construct three profiles along the propagation path (almost N-S) and three perpendicular to the propagation path (almost E-W) to look at the nature of propagation of these two types of surface waves. Groups of records from stations in various geological and tectonic provinces in California are also examined in order to establish regional characteristics of the surface waves. We find that the propagation characteristics of *Lg* differ from those of *Rg* across California; *Lg* waves are apparently more sensitive to crustal heterogeneities. The most striking observations are the similarity of coda for both the *Lg* and the *Rg* waves within geologic provinces and the marked difference in coda between regions. These differences are seen in the amplitudes, coda duration, shape of the energy envelope, frequency content, and sharpness of the phase initiation. In general, a decrease in the Moho depth near the Pacific Coast is correlated with a decrease in the surface wave amplitude, especially at higher frequencies (0.15-0.2 Hz). Most interesting is the association of the San Andreas fault with abrupt changes in the wave train amplitudes. The surface waves are amplified in the vicinity of the fault zone and then decrease in amplitude after the zone is crossed. In the Coast Ranges, amplitudes are low and waveform coherence is poor. The *Rg* phase dominates the record in the Sierra Nevada, and both surface waves are amplified by the thick sedimentary sequence of the Great Valley.

INTRODUCTION

The *Lg* and *Rg* phases were first recognized by *Press and Ewing* [1952] who described them as channel waves trapped in a granitic low-velocity zone at the base of the crust. The designations "*L*" and "*R*" derive from the transverse Love wave type particle motion and the retrograde elliptical Rayleigh wave type motion, respectively, that these two phases exhibit. The "*g*" signifies the granitic layer in which the waves were once thought to propagate. *Knopoff et al.* [1973] and *Levshin* [1973] demonstrated that Press and Ewing's simple model did not adequately explain these observationally complex phases and, furthermore, that a low-velocity zone is not required for the existence of *Lg* and *Rg* waves; a simple monotonically increasing shear velocity structure with depth is sufficient. For purely continental paths, *Lg* is often the most prominent phase on seismograms recorded at regional and intermediate (< 1000 km) distances within the 0.5- to 5-Hz frequency range. *Lg* does not, however, propagate across oceanic paths greater than 100 km [*Press and Ewing*, 1952]. Although the *Lg* wave has motion primarily in the horizontal plane, the phase also contains substantial components of vertical and radial motion, and thus it can be studied on vertical-component seismograms as we have done here. In general, the *Lg* phase has a group velocity of 3.51 ± 0.07 km/s (about the average crustal shear wave velocity) in the western United States [*Press and Ewing*, 1952], a period of 0.5-6 s, and exhibits reverse dispersion (higher frequencies have higher velocity) at $\Delta 20°$ from the source. *Lg* has been studied a great deal more than the *Rg* phase, which has a later arrival time. The *Rg* phase has a group velocity of 3.05 ± 0.07 km/s (about the average crustal Raleigh wave velocity) in the western United States [*Press and Ewing*, 1952] and an 8- to 12-s period. Both phases have durations up to several minutes, and *Ruzaikin et al.* [1977] and *Cara et al.* [1981] argued that this characteristic can only be reasonably explained by multipathing, scattering, and mode conversions caused by lateral inhomogeneities. The *Lg* coda is largely affected by the propagation path and receiver site and is not strongly influenced by the source mechanism [*Gregerson*, 1984; *Campillo*, 1986].

The *Lg* and *Rg* phases have been successfully modeled as a superposition of fundamental and higher-mode surface waves propagating within the crustal waveguide [e.g., *Knopoff et al.*, 1973; *Cara and Minster*, 1981; *Bouchon*, 1982; *Herrmann and Kijko*, 1983; *Kennett*, 1985]. Other studies using *Lg* and *Rg* include those involving spatial attenuation, magnitude scaling and underground nuclear explosion yields [e.g., *Nuttli*, 1986, 1973; *Campillo*, 1987; *North*, 1985; *Campillo et al.*, 1985; *Shin and Herrmann*, 1987], lateral anisotropy effects [e.g., *Kafka and Reiter*, 1987; *Kennett*, 1986], and observational analyses [e.g. *Båth*, 1954; *Gregerson*, 1984; *Der et al.*, 1984; *Ruzaikin*, 1977; *Kafka and Reiter*, 1987]. Data analyses are difficult due to the many factors which affect the *Lg* and *Rg* phases, and not all studies are in agreement. Most studies, however, do agree that local and regional geology can have a significant effect on the *Lg* and *Rg* waveform characteristics [*Rivers*, 1980; *Der et al.*, 1981; *Campillo*, 1987].

In this study we use the December 23, 1985, Nahanni, Canada, earthquake as recorded on the central and south-

Paper number 91JB00920.
0148-0227/91/91JB-00920$05.00

ern California regional networks. The reasons for choosing this particular event are that it was recorded on most of the stations and that its shallow hypocentral depth, large magnitude (M_S 6.9), intermediate distance to California, and purely continental path resulted in good *Lg* and *Rg* waves with which to do a comprehensive study. The epicenter is 2267 km away from the northernmost station in the Central California Network and 3098 km away from the southernmost station used in this study (Figure 1).

Since all the short-period instruments in the California regional networks are nominally identical, we corrected only for individual station gains (rather than the correcting for the entire instrument response). Consequently, this is not intended to be a detailed quantitative analysis of *Lg* and *Rg*; rather it is a descriptive presentation and summary of a large *Lg* and *Rg* data set recorded on the short-period networks in California. We attempt to correlate the crustal geology and structure with the various features in the wave trains.

CALIFORNIA REGIONAL NETWORK DATA

The regional networks in California were originally designed for the purpose of locating regional earthquakes and determining magnitudes. The network instruments are all short-period velocity seismometers with a natural period of 1-s and, with the exception of a few stations, record only vertical motions. In this study we use only vertical component seismograms. The Central California Network has about 300 stations, and the Southern California Network has about 250 stations. Both networks are monitored with the California Institute of Technology-U.S. Geological Survey (Caltech-USGS) Seismic Processing System (CUSP) digital recording system [*Johnson*, 1983; *Given et al.*, 1987]. In addition to digital recording, frequency modulation (FM) analog tapes continuously record most stations in the networks as a backup to the real-time processing system. Since the digital recordings do not include the surface wave portion of teleseismic events and often do not trigger on teleseismic events, we obtained the Nahanni data from the FM analog tapes.

We use 15 min of data from approximately 200 stations, most of which are part of the Central California Network. The records are band-pass filtered from 0.01 to 1.0 Hz using a zero-phase Butterworth filter and then decimated to 5 samples/s for use in the study. The lack of complete infor-

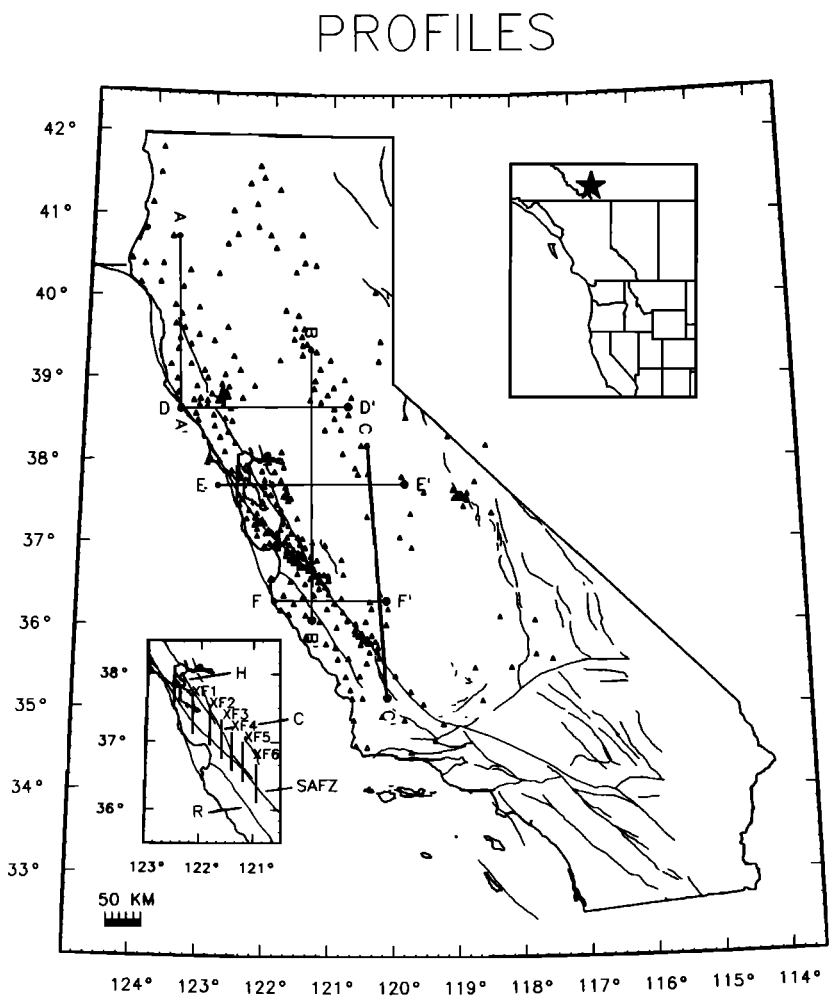

Fig. 1. Map of California showing profiles presented in this study. A-A′, B-B′, and C-C′ are parallel to the propagation direction, and D-D′, E-E′, and F-F′ are perpendicular. The inset in the upper right shows the location of the Nahanni earthquake, indicated by a star. The inset in the lower left shows the profiles across the San Andreas fault. Stations are shown as triangles. Abbreviations are H, Hayward fault; C, Calaveras fault; SAFZ, San Andreas fault zone; R, Rinconada fault.

mation about the instruments at the time of the earthquake did not permit us to remove the entire instrument response with confidence; however, we were able to correct for the gain of each instrument. This correction allowed us to obtain the nominal instrument response and use relative amplitude information since all the instrument response curves are nominally the same. We did not carry out an independent check on the station responses; therefore, although we use the apparent amplitudes as if they were real, some anomalous amplitudes may be the result of incorrect gain information. We make interpretations only in the cases where systematic correlations lead us to believe the amplitudes are reflecting a real variation.

Since the instrument response has not been entirely removed from the data, it is important that we understand what that response is and how it affects the waveforms. Figure 2 represents the theoretical instrument response of the 1-Hz short-period seismometers with the two most commonly used discriminator types at a variety of attenuation settings. The amplitude response is proportional to ω^3 below 1 Hz. Although the curves in Figure 2 look different at high frequencies for the two discriminators, note that the curves are almost identical for frequencies below 1 Hz, which is the region that applies to the data in this study. The effect of this instrument response on our data is that the *Lg* waves are recorded at a higher amplitude than the longer-period *Rg* waves, even though the ground displacement from the *Rg* waves may, in fact, be greater. We cannot be sure that an anomalous amplitude is not due to a deviation in the natural frequency of the instrument, which would particularly affect the low-frequency *Rg* waves. The two amplitude values for *Lg* and *Rg* beside each record in the figures have also been corrected for distance based on Δ^{-3} for *Lg* and Δ^{-1} for *Rg* as seen in Figure 11 and is discussed later.

The station spacing of the network ranges from about 1 to 50 km, and our profiles have an average station spacing of about 25 km. The length of our profiles varies from about 150 to 350 km. The duration of the *Lg* and *Rg* coda varies from region to region, but the typical duration is about 2-3 min for *Lg* waves and at least 4-5 min for *Rg* waves. The onset of these phases is emergent in most cases, making it difficult to assign a time to the arrival of the wave group. In this study we assign arrival times as those predicted using the velocities as described by *Press and Ewing* [1952]. In addition, the complete *Rg* coda was not on the data tapes we used, and as a result we were unable to determine the length of the *Rg* wave train with certainty. The *Lg* waves in this study have a dominant period of about 1.5-3.5 s on the network instruments, and the *Rg* waves have a dominant period of about 6.5-9 s.

METHOD

We constructed many profiles during the study; however, we present only three N-S profiles and three E-W profiles here based on the best station coverage. All the records shown in the figures have been further band-pass filtered from 1 to 15 s using a zero-phase Butterworth filter in order to minimize noise. The amplitudes shown and referenced are the average *Lg* amplitude and the average *Rg* amplitude recorded on the short-period instrument and corrected for gain. The average amplitudes were determined using a 150-s window starting approximately 30 s into the wave train for the *Lg* waves and using a 180-s window starting at the end of the *Lg* window for the *Rg* waves. It was found that varying the time windows up to 30 s did not change the amplitudes by more than about 0.02 units. The average of the absolute amplitude of the digital seismogram in the

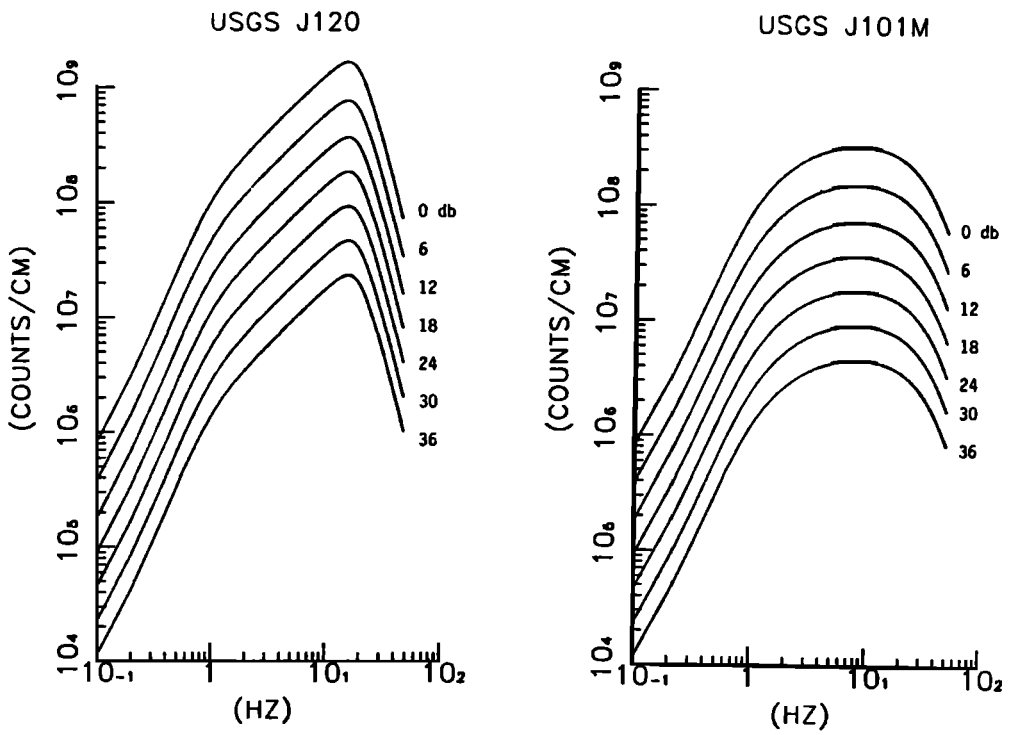

Fig. 2. Instrument response for the 1-Hz seismometer with a J120 and a J101M discriminator, two of the most commonly used discriminators in the network, at various attenuation settings.

window was taken to determine the average amplitude. It is important to remember that these are narrow-band seismograms and not absolute ground motions. The values are only relative amplitudes of the seismograms (corrected for gain) and therefore do not have any units. All records with amplitudes of 2.5 or greater have been normalized to 2.5 in the figures.

The information used to construct the geologic profiles accompanying the waveforms in Figures 3-8 was compiled from *Oppenheimer and Eaton* [1984], *Walter and Mooney* [1982], *Colburn and Mooney* [1986], *Eaton* [1963], *Mavko and Thompson* [1983], and *Zucca et al.* [1986].

In attempting to explain the characteristics of the surface wave coda and the propagation patterns, we have considered the receiver site attributes and the propagation path structure including site geology, crustal thickness, and sediment depth, as well as faults and other abrupt lateral variations. We have also compared the behavior of the *Lg* wave train with that of the *Rg* wave train.

PROFILES

The following are descriptions of profiles A-A′ through F-F′, the locations of which are shown in Figure 1.

A-A′

A-A′ shown in Figure 3, is parallel to the propagation direction and diagonally crosses the north Coast Ranges, terminating at the Pacific coast. This profile spans a large section of the Franciscan assemblage including the Central belt (a melange with mostly graywackes and metagraywackes) and the Coastal belt (arkosic sandstones) [*Blake and Jones*, 1981]. There is no recognizable difference in the wave trains between these two belts, but there is a gradual decrease in amplitude toward the coastline (*Lg* decreases from 0.5 to 0.3; *Rg* decreased from 0.2 to 0.1). This decrease in amplitude for stations on the coastline is seen generally on all stations along the Pacific coast in this study. The onset of *Lg* is not sharp on most of the records, and the average *Lg* amplitude is moderate compared to other profiles. The *Rg* phase is not pronounced in these records. The first 40 s of the *Lg* wave train includes some 0.15- to 0.2-Hz energy, longer period than the rest of the *Lg* coda with the exception of KPP and KKP, the two stations farthest inland on this profile.

B-B′

Profile B-B′, shown in Figure 4, is also parallel to the direction of propagation. It crosses the metamorphic foothill belt of the northern Sierra Nevada [*Bateman*, 1981], extends through the central Great Valley and the Salinian block of the north Coast Ranges near Monterey Bay [*Page*, 1981], and terminates at the coastline south of the bay. Unfortunately, there are no stations in the Great Valley, and we have no data on the transition from the Sierra Nevada to the Coast Ranges. A remarkable difference in the appearance of the wave trains between these two areas can be seen both in the more pronounced *Rg* waves in the Sierra Nevada (due to less high-frequency energy content) and the slightly higher (0.1 units higher) average *Lg* peak amplitude in the Coast Ranges east of the San Andreas fault.

The San Andreas and Calaveras fault zones coincide with dramatic changes in the waveforms in this profile. Station HPH is located in the fault zone and has a very high amplitude for both *Lg* and *Rg*. All the stations west of the fault, on the granitic and metamorphic Salinian block, have a greatly diminished amplitude relative to those on the east side (Franciscan terrane). In this case, the abrupt decrease in amplitudes in coastal areas appears to be related to the fault zone, in contrast to the more gradual decrease in amplitudes seen in profile A-A′ toward the coast. Other stations in the area also exhibit this significant change in amplitude.

C-C′

Profile C-C′, shown in Figure 5, is the easternmost profile along the propagation path. It begins in the foothill belt of the Sierra Nevada, [*Bateman*, 1981] and spans both the Great Valley and the Salinian block of the south Coast Ranges [*Page*, 1981]. This profile can be separated into three distinct groups based on the appearance of the *Lg* and *Rg* waveforms. The three stations in the Sierra Nevada have relatively sharp *Rg* arrivals and clear wave trains unobscured by the higher-frequency energy of the *Lg* phase. The next group of stations is located on the edge of the Great Valley, and the most noticeable feature of the group is the high amplitude of both surface wave groups. Here, the high-frequency energy of the *Lg* phase lasts well into the arrival of the *Rg* phase. The station west of the San Andreas fault zone has a much smaller amplitude for both *Lg* and *Rg* waves than stations east of the fault zone.

D-D′

Profile D-D′, shown in Figure 6, is the northernmost profile perpendicular to the direction of propagation. It trends from the Pacific coast north of San Francisco (Coastal and Central belts of the Franciscan assemblage) [*Blake and Jones*, 1981], across the Great Valley to the metamorphic foothill belt of the Sierra Nevada [*Bateman*, 1981]. The most noticeable difference between the E-W profiles and the N-S profiles is the lack of interstation coherence in the energy groups seen on the E-W profiles in a qualitative sense. This is an indication that heterogeneities in the propagation path produce scattering or changes in the phase velocity [*Der et al.*, 1984]. The records nearest to the coast contain low-frequency energy at the initiation of the *Lg* wave similar to that on profile A-A′. The records on either side of the Great Valley have anomalously large amplitudes. The *Rg* wave on the record in the Sierra Nevada dominates much earlier than those in other regions.

E-E′

Profile E-E′, shown in Figure 7, trends perpendicular to the propagation direction from the Pacific coast, across San Pablo Bay, the Great Valley, and the metamorphic foothill belt of the Sierra Nevada [*Bateman*, 1981]. Station MAT (farthest east) is within the granitic batholith of the Sierra Nevada. Three distinct groups of records can be seen on this profile. Starting from the west, the record near the coast has a low amplitude (approximately 0.1 units). Stations CSP, CBW, CRP, and CAC on the broken Franciscan terrane, have high amplitudes (> 0.3 units) and pronounced *Rg* wave trains. The three records in the Sierra Nevada once again have high average amplitudes and a pronounced *Rg* wave train.

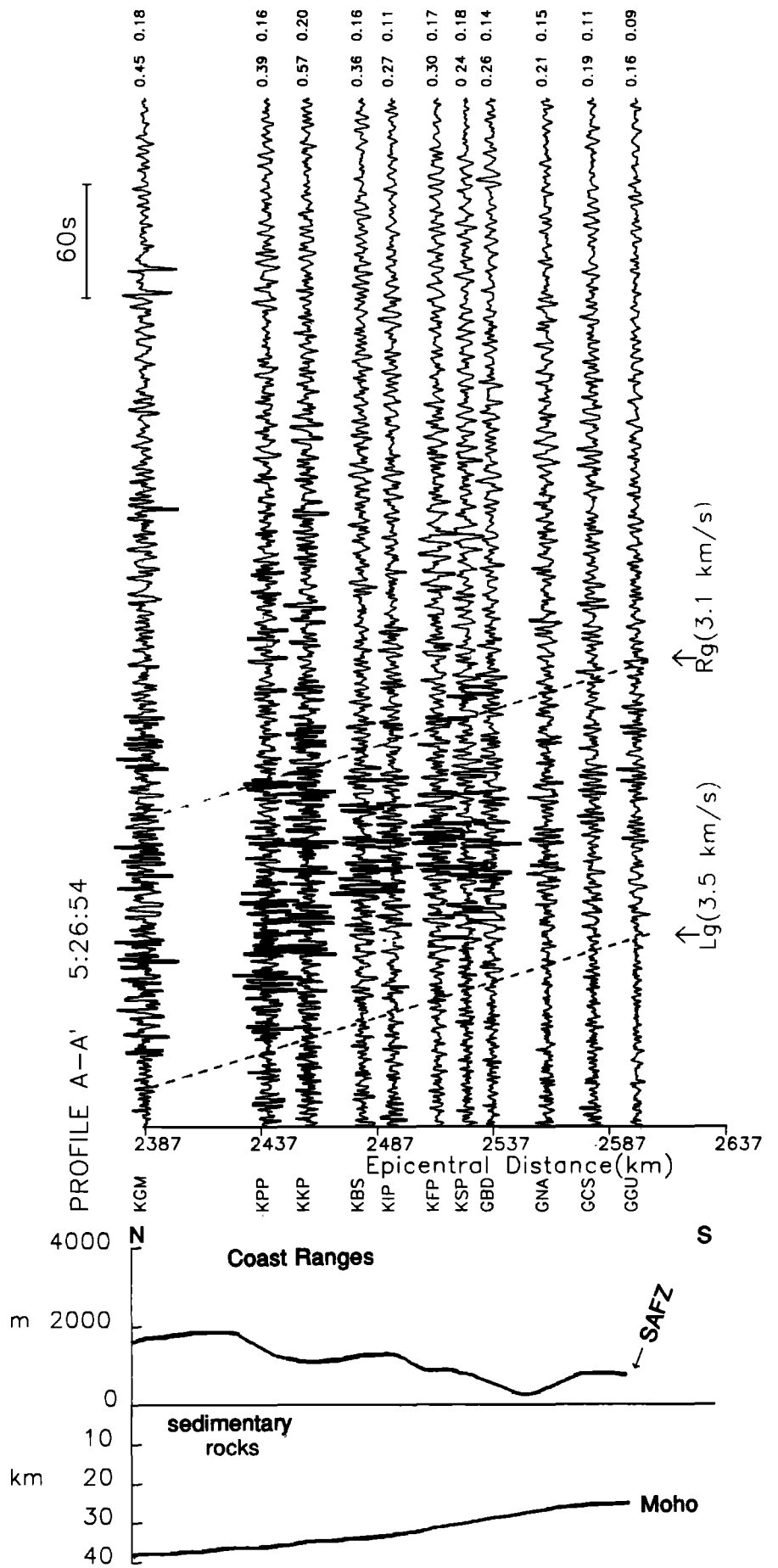

Fig. 3. Profile A-A'. The dashed lines represent the approximate *Lg* and *Rg* group arrival times. The average *Lg* and *Rg* amplitudes are shown to the right of each seismogram. The sketch of the geologic cross section shows corresponding structure beneath the stations. Note the difference in scale between topography and subsurface structure. SAFZ is San Andreas fault zone.

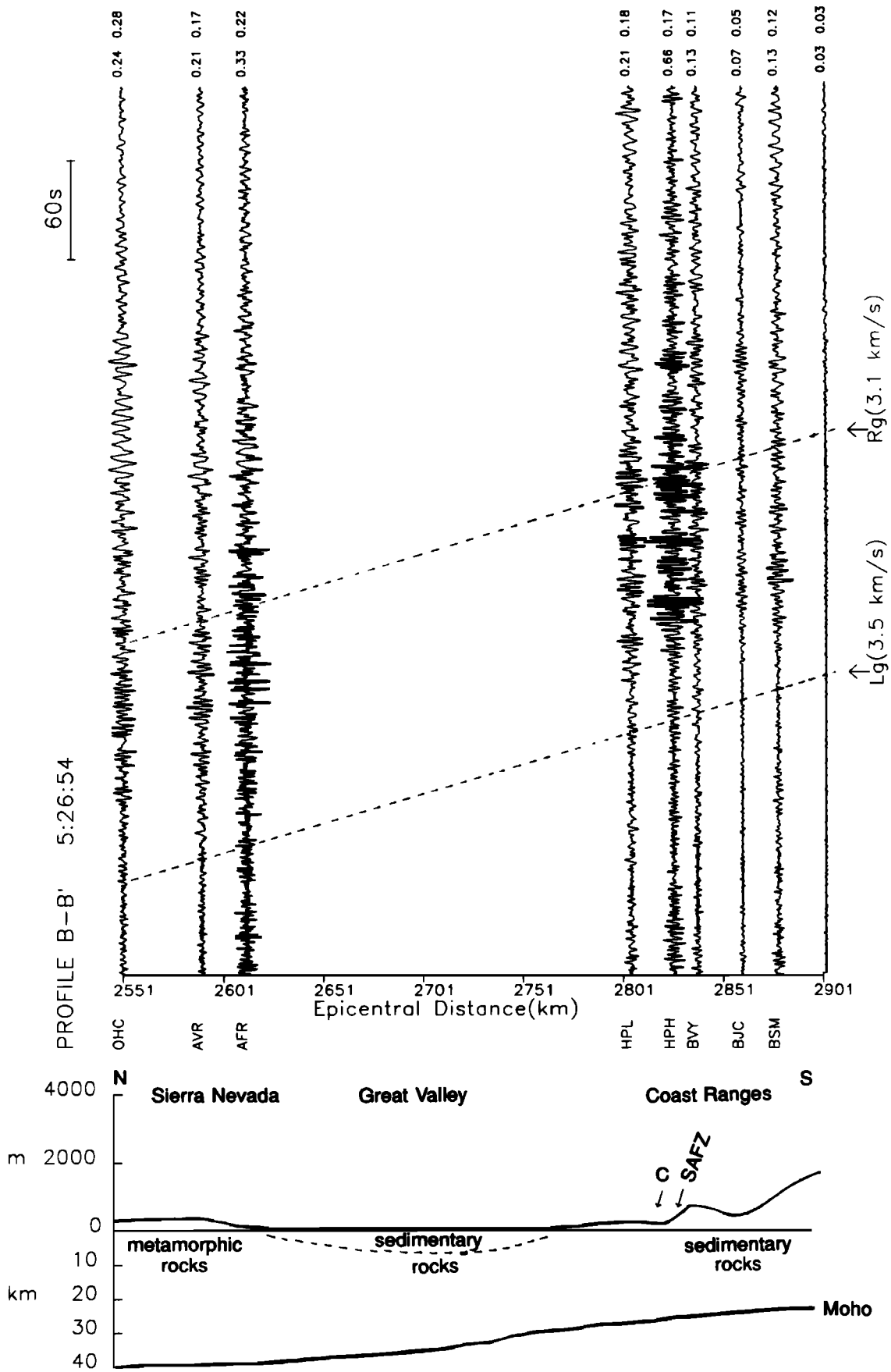

Fig. 4. Profile B-B'. The dashed lines represent the approximate *Lg* and *Rg* group arrival times. The average *Lg* and *Rg* amplitudes are shown to the right of each seismogram. The sketch of the geologic cross section shows corresponding structure beneath the stations. Note the difference in scale between topography and subsurface structure. SAFZ is San Andreas fault zone, and C is Calaveras fault.

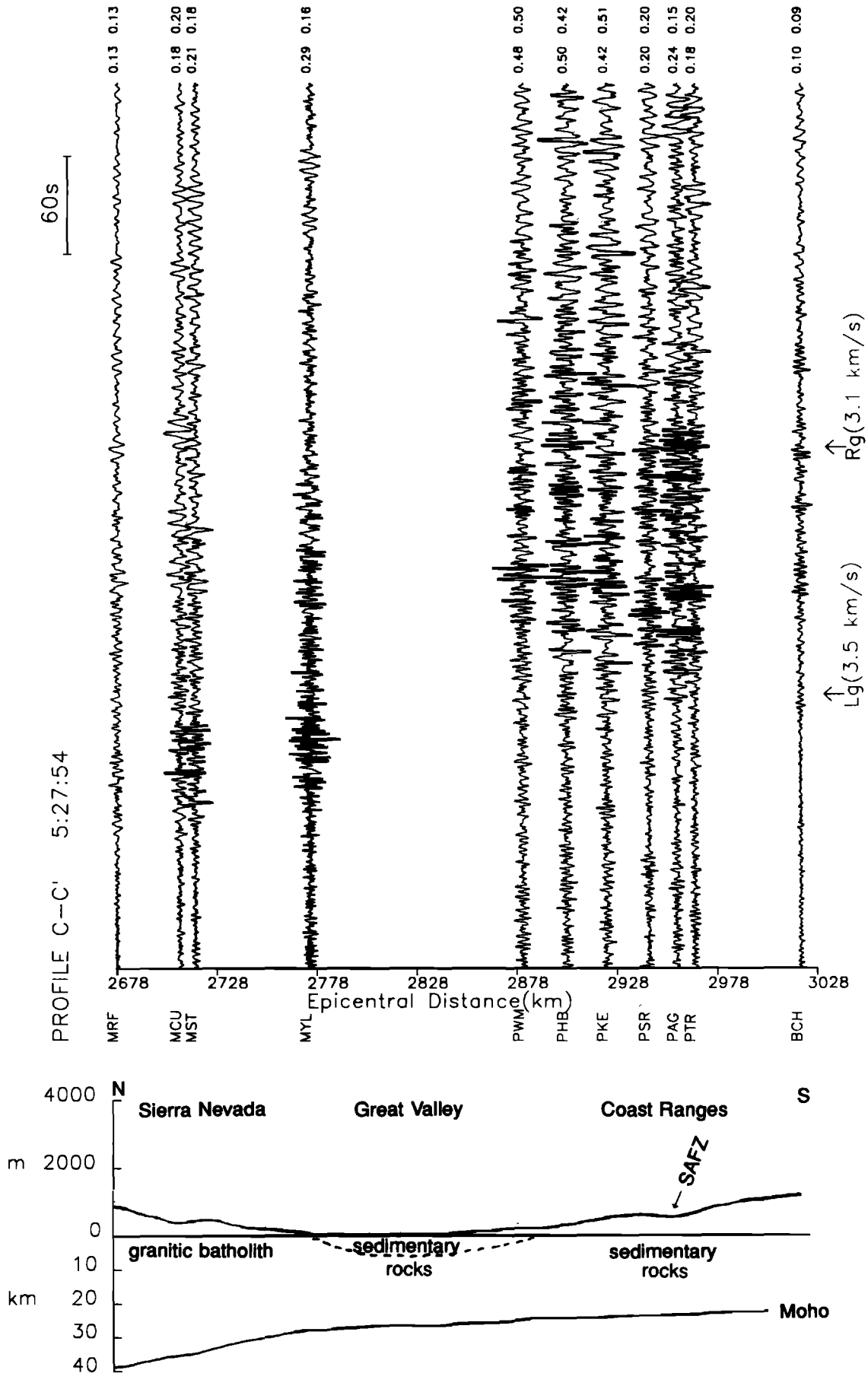

Fig. 5. Profile C-C'. The dashed lines represent the approximate *Lg* and *Rg* group arrival times. The average *Lg* and *Rg* amplitudes are shown to the right of each seismogram. The sketch of the geologic cross section shows corresponding structure beneath the stations. Note the difference in scale between topography and subsurface structure. SAFZ is San Andreas fault zone.

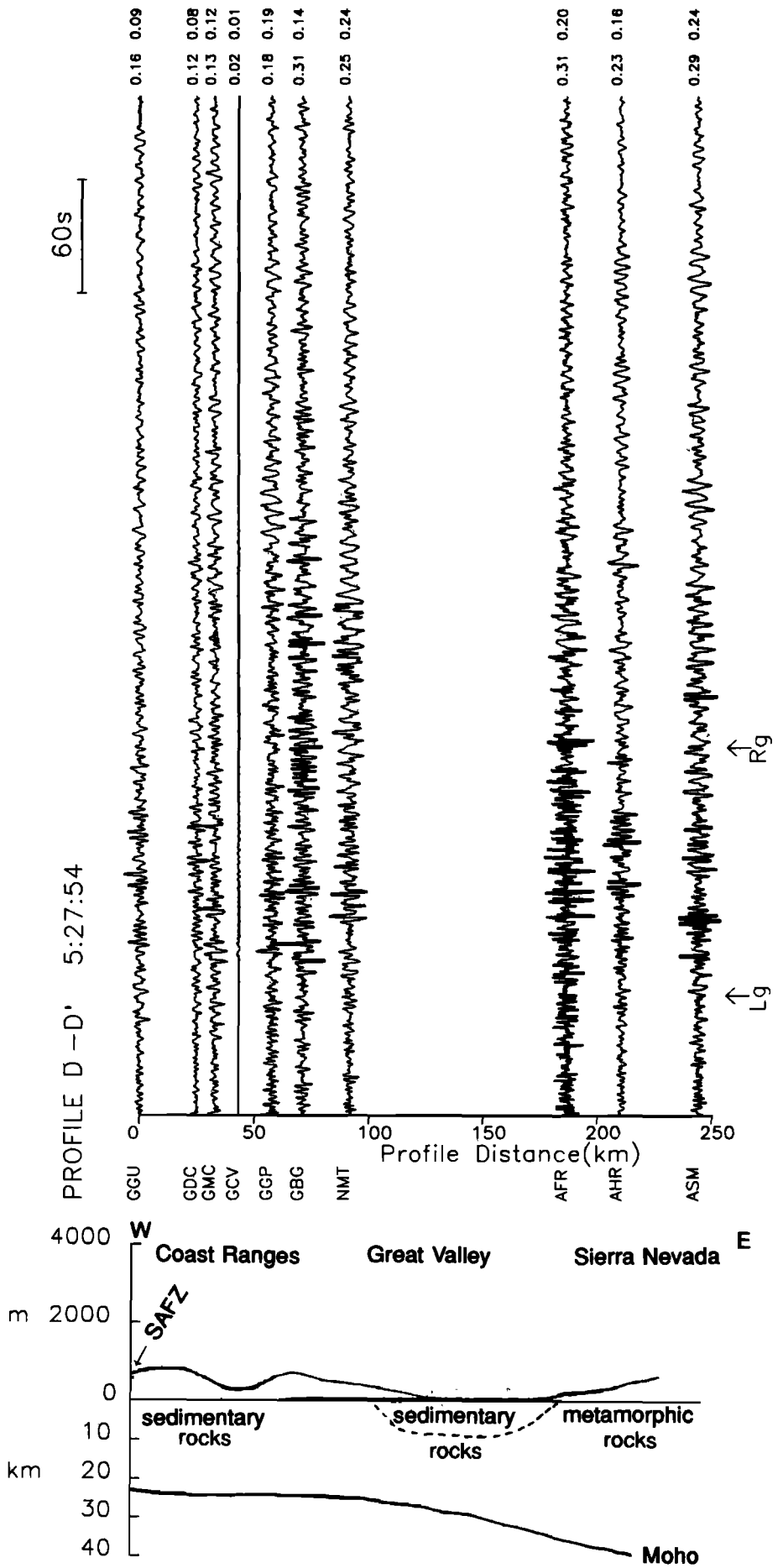

Fig. 6. Profile D-D'. *Lg* and *Rg* group arrival times are indicated. The average *Lg* and *Rg* amplitudes are shown to the right of each seismogram. The sketch of the geologic cross section shows corresponding structure beneath the stations. Note the difference in scale between topography and subsurface structure. SAFZ is San Andreas fault zone.

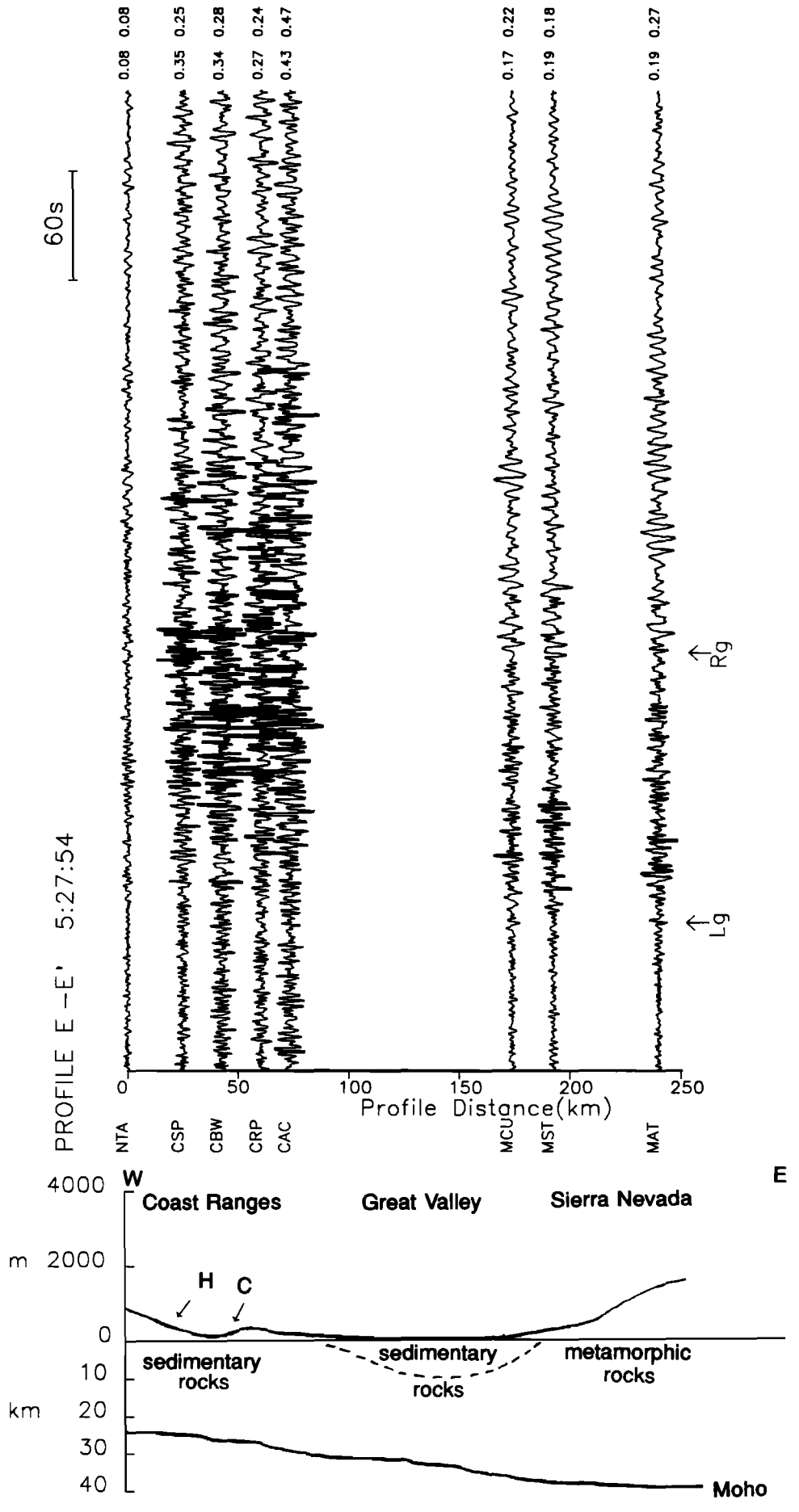

Fig. 7. Profile E-E'. *Lg* and *Rg* group arrival times are indicated. The average *Lg* and *Rg* amplitudes are shown to the right of each seismogram. The sketch of the geologic cross section shows corresponding structure beneath the stations. Note the difference in scale between topography and subsurface structure. H is Hayward fault, and C is Calaveras fault.

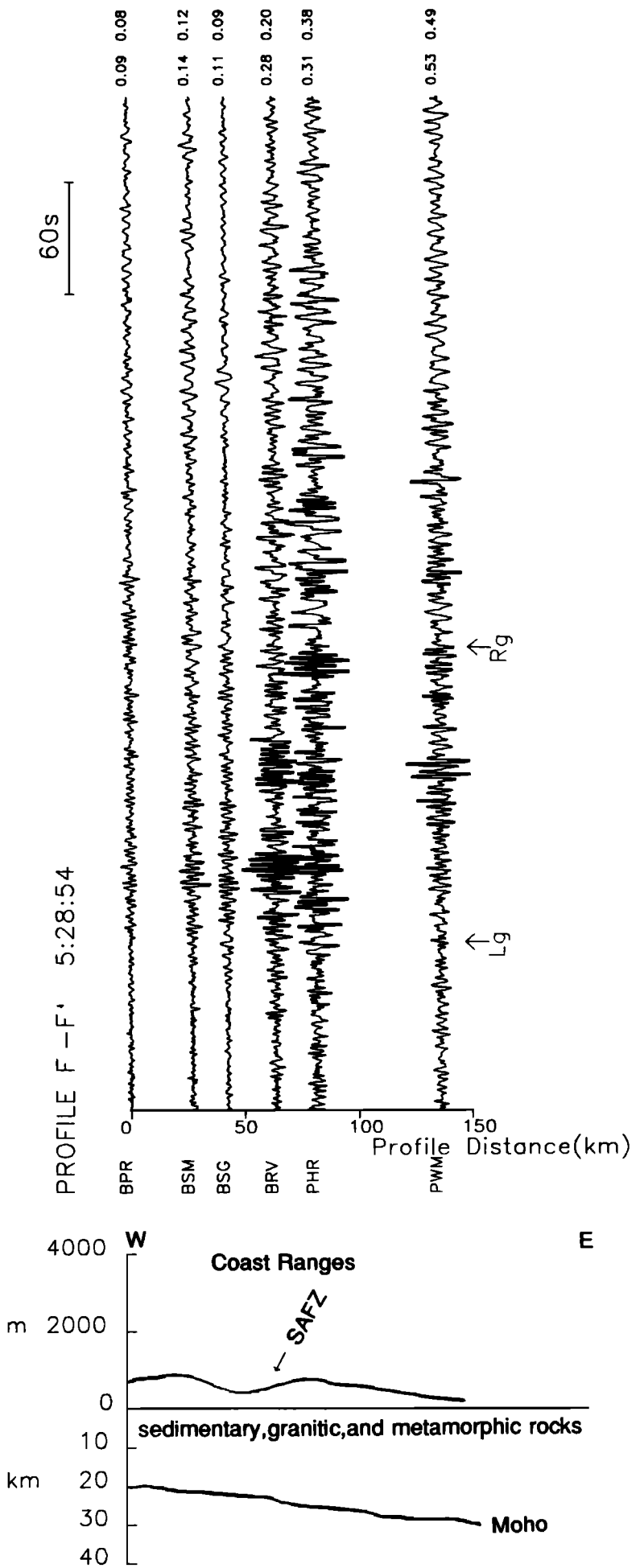
60s
PROFILE F–F' 5:28:54
0.09 0.08
0.14 0.12
0.11 0.09
0.28 0.20
0.31 0.38
0.53 0.49
Rg
Lg
0
50
100
150
Profile Distance(km)
BPR
BSM
BSG
BRV
PHR
PWM
W
E
4000
m 2000
0
Coast Ranges
SAFZ
sedimentary,granitic,and metamorphic rocks
10
km 20
30
40
Moho

F-F'

Profile F-F', shown in Figure 8, is also perpendicular to the propagation direction. It begins at the Pacific coastline and crosses the Salinian block [*Page*, 1981] and Franciscan assemblage [*Blake and Jones*, 1981] in the south Coast Ranges just south of Monterey Bay, ending at the west edge of the Great Valley. The San Andreas fault once again separates low amplitudes, associated with the Franciscan terrane to the east, from higher amplitudes, associated with the Salinian block, to the west.

Profiles Across the San Andreas Fault

Figure 9 shows six short approximately N-S profiles that were constructed across the San Andreas fault zone parallel to the propagation path to investigate the effect of the fault on the surface waves (the locations of these profiles are shown in Figure 1). Most profiles are about 50 km in length. The amplitude values for *Lg* and *Rg* beside each record in these profiles have not been corrected for distance; the 50-km range changes the amplitudes by less than about 5%, which is beyond the resolution of the amplitudes in this study. All the profiles show an increase in amplitude (especially *Lg*) in the vicinity of the San Andreas fault followed by a decrease in amplitude south of the fault (after the fault is crossed from north to south).

Figures 10*a*-10*e* show the *Lg* and *Rg* amplitude changes along these profiles as they cross both the Calaveras fault (in some cases) and the San Andreas fault. Profiles XF2 and XF3 are plotted separately from the others because they

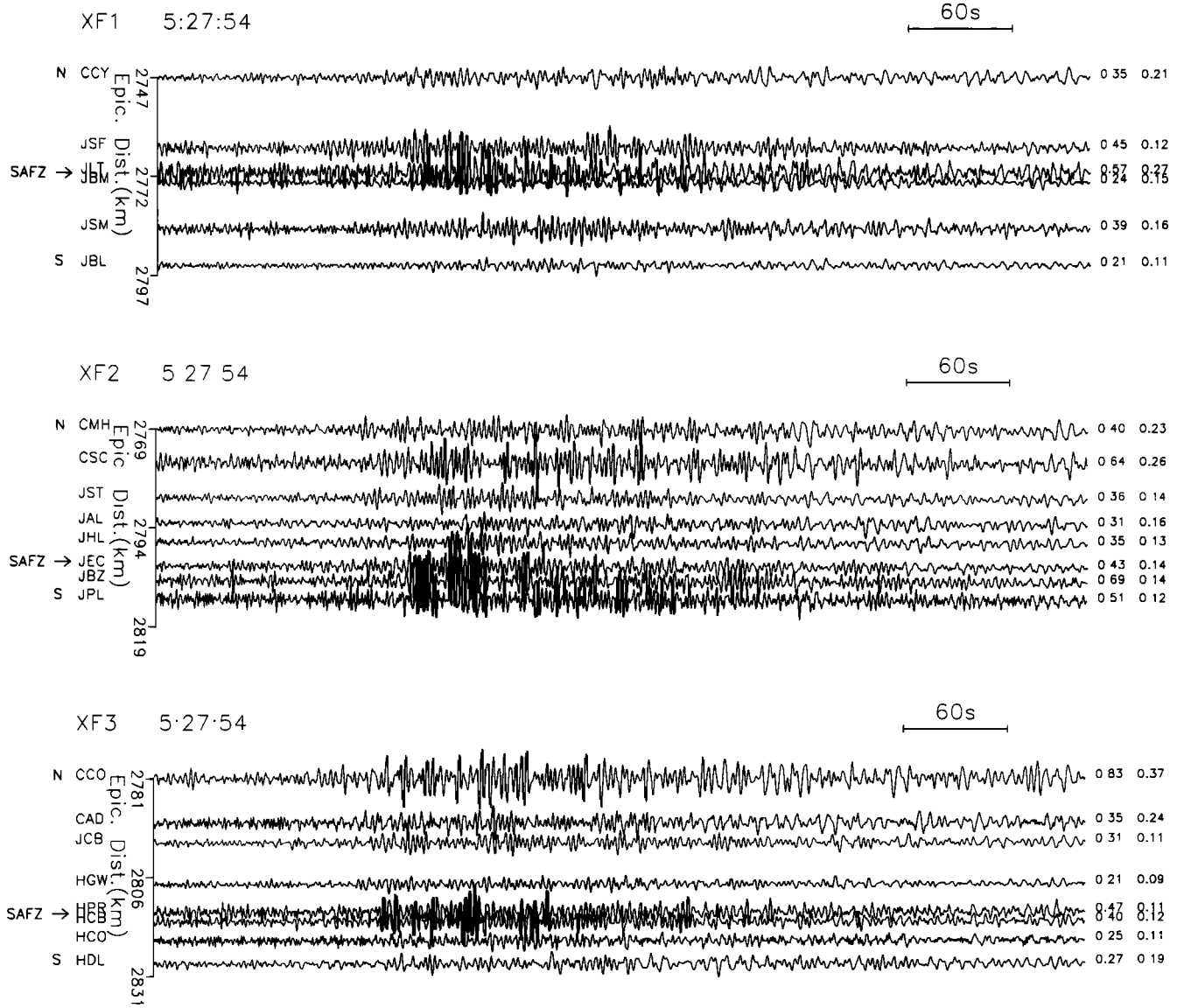

Fig. 9. Short (50 km) profiles across the San Andreas fault. Location of the San Andreas fault zone (SAFZ) is shown. Profiles are approximately N-S.

Fig. 8. Profile F-F'. *Lg* and *Rg* group arrival times are indicated. The average *Lg* and *Rg* amplitudes are shown to the right of each seismogram. The sketch of the geologic cross section shows corresponding structure beneath the stations. Note the difference in scale between topography and subsurface structure. SAFZ is San Andreas fault zone.

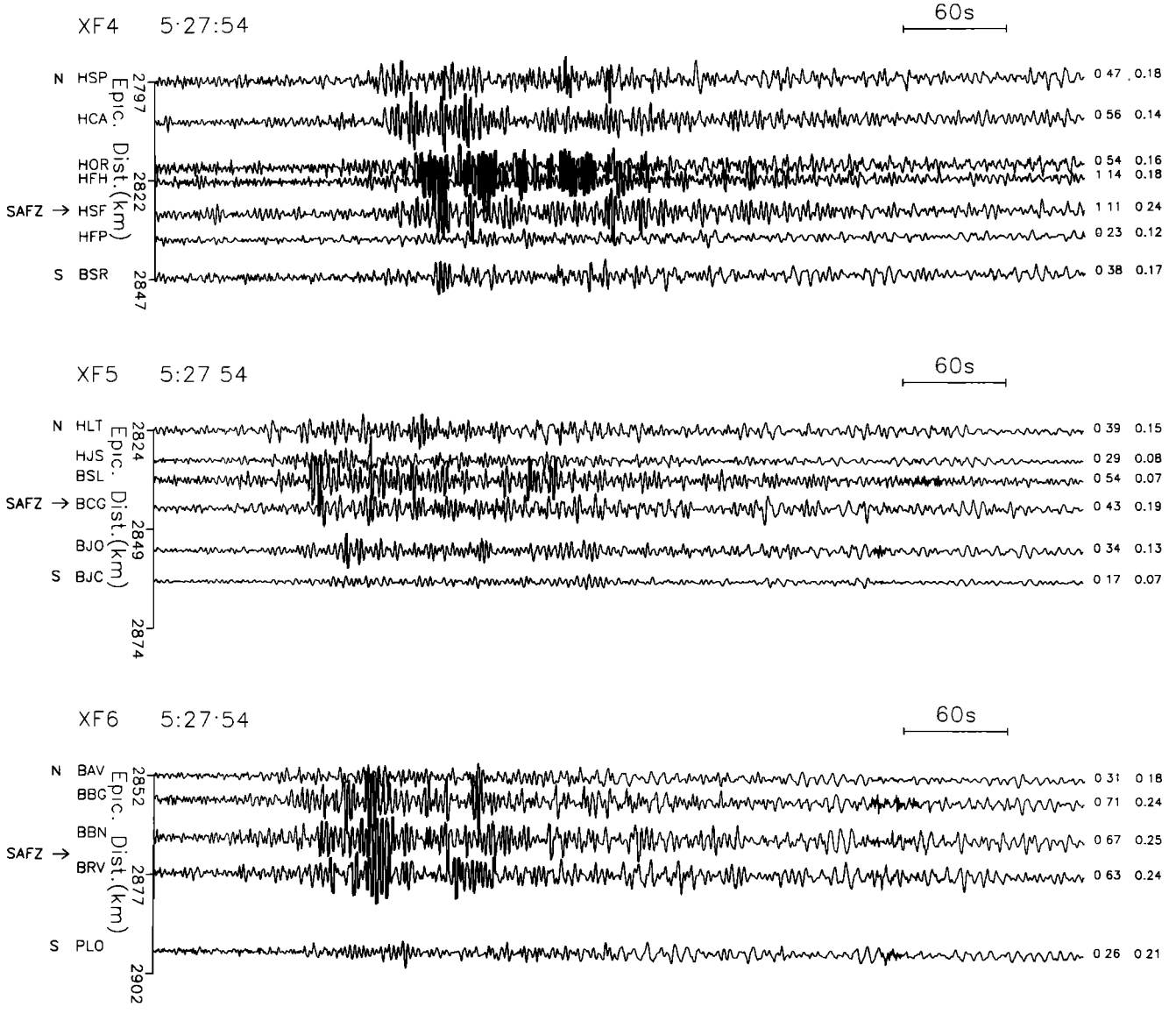

Fig. 9. (continued)

have a slightly different amplitude profile. All *Lg* profiles show an increase in amplitude near the San Andreas fault, and those crossing the Calaveras fault also show an increase in that area. XF1, XF4, XF5, and XF6 (Figure 10*a*) have a gradual rise in *Lg* amplitude, peaking at the San Andreas fault, followed by a sharp drop in amplitude after the fault is crossed. XF2 and XF3 (Figure 10*b*), on the other hand, have high *Lg* amplitudes at the Calaveras fault that decrease after the fault is crossed, followed by another increase in amplitude that occurs just after the San Andreas fault is crossed.

The *Rg* profiles are somewhat different. XF2 and XF3 (Figure 10*d*) show an increased amplitude at the Calaveras fault, followed by a decrease. The amplitude does not increase at the San Andreas fault on these two profiles. XF1, XF4, XF5, and XF6 (Figure 10*c*), however, do show a gradual rise in amplitude approaching the San Andreas fault with a peak at the fault, followed by a sharp decrease in amplitude after the fault is crossed. Differing crustal structure along the length of the faults, or perhaps the varying proximity of the faults themselves, appears to have an effect on the amplitude variations of the seismograms. Profiles XF2 and XF3 cross both the Calaveras and the San Andreas faults and look similar. However, XF1, XF4, XF5, and XF6 have a different amplitude variation pattern. These three profiles cross only the San Andreas fault (see Figure 1). XF1 crosses the Hayward fault and the southern tip of the San Francisco Bay before reaching the San Andreas fault, so those surface waves may have further complications.

The plot of the average values of all profiles (Figure 10*e*) shows a rather dramatic increase in amplitude for *Lg* waves at the approach to the San Andreas fault followed by a sharp decrease and yet another much smaller increase in amplitude at the Rinconada fault. The amplitude variation for *Rg* waves mirrors that of the *Lg* waves but is more subtle. Additional data were added at the SW end of profiles XF3, XF4, XF5, and XF6 for this plot in order to observe the amplitude variation at the Rinconada fault.

On a larger scale, Figure 11 represents the average *Lg* and *Rg* amplitudes across California from north to south. The 17 data points that make up each curve were derived by calculating the average amplitude of all the seismograms

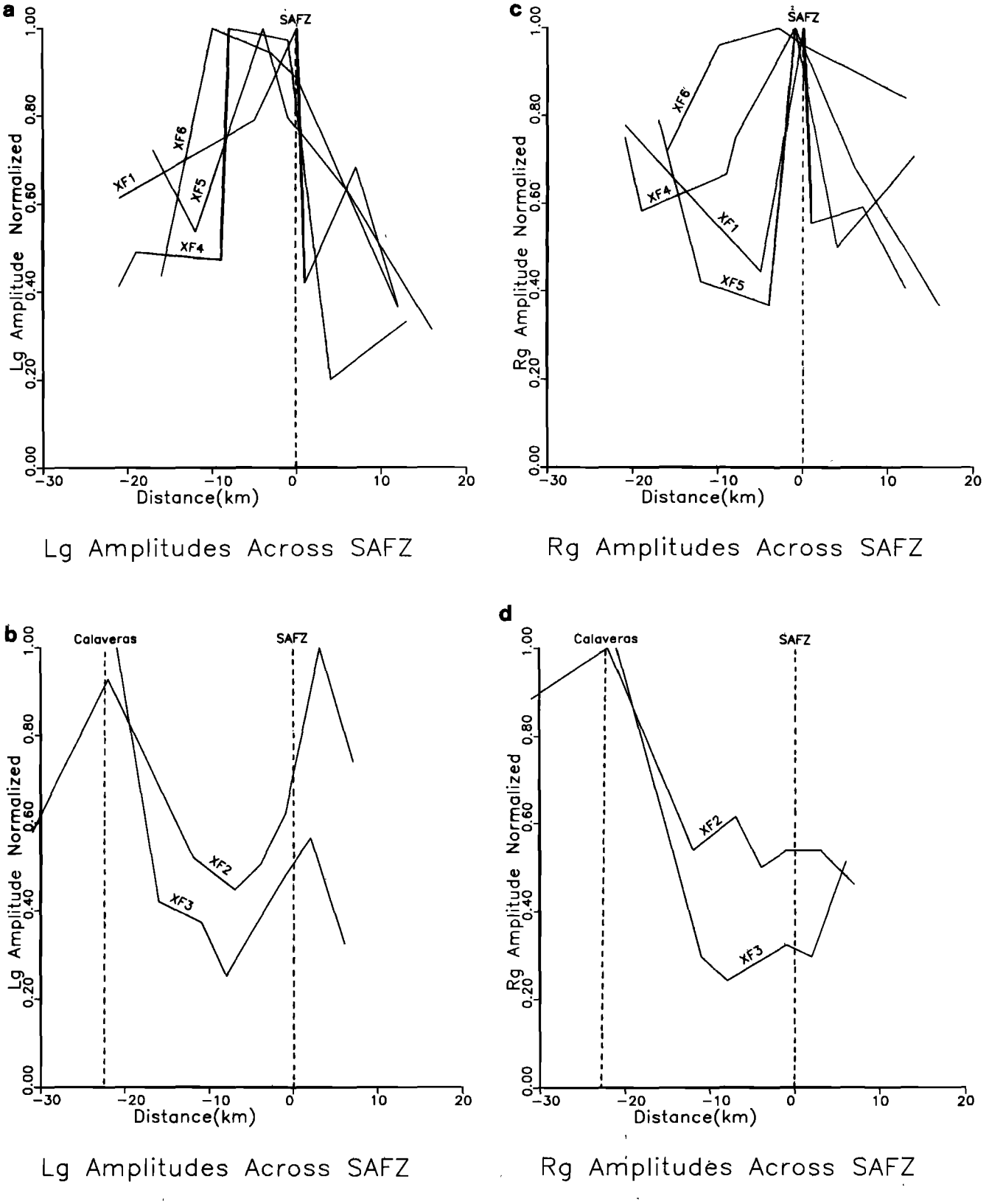

Fig. 10. *Lg* and *Rg* amplitudes across the San Andreas fault. Locations of the profiles XF1 through XF6 are shown in Figure 1. (*a*) Normalized *Lg* amplitudes for profiles XF1, XF4, XF5, and XF6. These profiles (except XF1) cross the San Andreas fault only. (*b*) Normalized *Lg* amplitudes for profiles XF2 and XF3. These profiles cross both the Calaveras fault and the San Andreas fault. (*c*) Normalized *Rg* amplitudes for profiles XF1, XF4, XF5, and XF6. These profiles (except XF1) cross the San Andreas fault only. (*d*) Normalized *Rg* amplitudes for profiles XF2 and XF3. These profiles cross both the Calaveras fault and the San Andreas fault. (*e*) Average of *Lg* amplitudes and *Rg* amplitudes for all profiles. Additional data was added to the SW end in order to extend the profile line across the Rinconada fault.

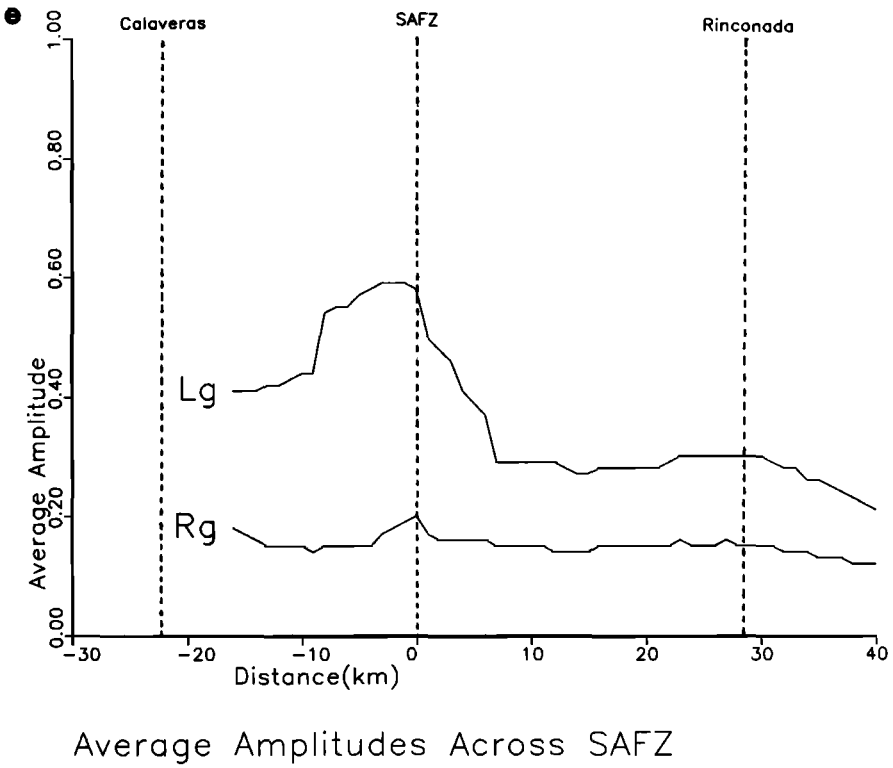

Fig. 10. (continued)

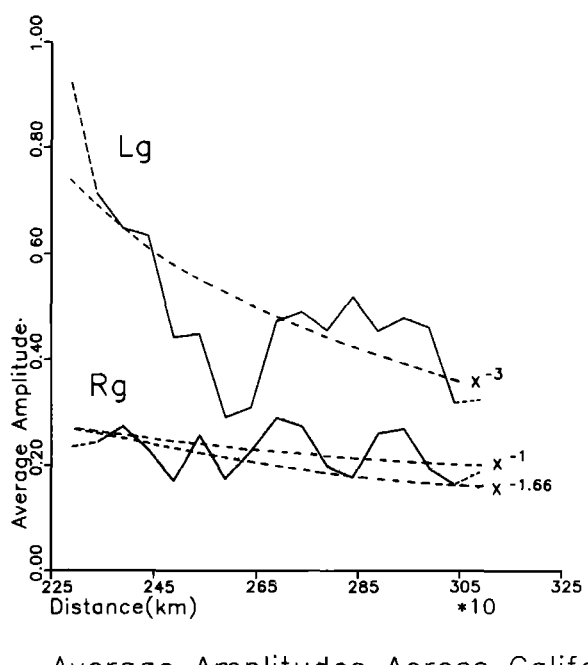

Fig. 11. Profile of average *Lg* and *Rg* amplitudes across California. The 17 data points were determined by taking 50-km-wide "bands" of California from north to south and calculating the average amplitude from all the recorded seismograms within each respective band. The first and last legs of the curves are dashed because they were based on only three and four stations, respectively. The smooth dashed curve associated with the *Lg* data is the predicted amplitude decay of 1-Hz *Lg* waves in the western United States from *Der et al.* [1984]. The two smooth dashed curves associated with the *Rg* data are the $\Delta^{-1.66}$ distance correction for 20-s Rayleigh waves from *Okal* [1989], and the best-fitting curve of Δ^{-1}.

recorded within 50-km-wide "bands" (equidistant from the Nahanni epicenter) of California from north to south at regular intervals. All bands contain from 5 to 43 stations (average of 19), with the exception of the northernmost and southernmost bands which contain only three and four stations, respectively. The first and last legs of the curves are dashed as a result. The smooth dashed curve associated with the *Lg* data is the predicted amplitude decay of 1-Hz *Lg* waves in the western United States after *Der et al.* [1984] (Δ^{-3}) and seems to fit the data reasonably well. The *Rg* data set has two curves associated with it in Figure 11. The $\Delta^{-1.66}$ curve is the theoretical distance correction for 20-s Rayleigh waves in the range 20°-160° as determined by *Okal* [1989]. This figure depends on factors such as dispersion and attenuation. Although our data set does not cover a large enough distance to resolve an *Rg* amplitude decay figure with certainty, it appears that the Δ^{-1} curve, rather than the $\Delta^{-1.66}$ curve, is the best fitting approximate curve to the data.

Lg AND *Rg* WAVES IN DIFFERENT REGIONS

We have taken seven groups of stations from different geologic areas (see Figure 12, after the 1983 map of O. P. Jenkins as presented by *Hinds* [1952]), including the Klamath Mountains, the Sierra Nevada, the Cascade Range, the north and south Coast Ranges, the Great Valley, and the Mammoth area, in order to investigate the characteristics of *Lg* and *Rg* coda within each area and to compare the similarities and differences in the wave trains between areas. Again, only relative amplitude ratios between regions are informative without the removal of the entire instrument response. Figures 13 and 14 provide a summary of the distribution of *Lg* and *Rg* amplitudes in California, and Figure 15 shows the characteristic codas from each of the regions.

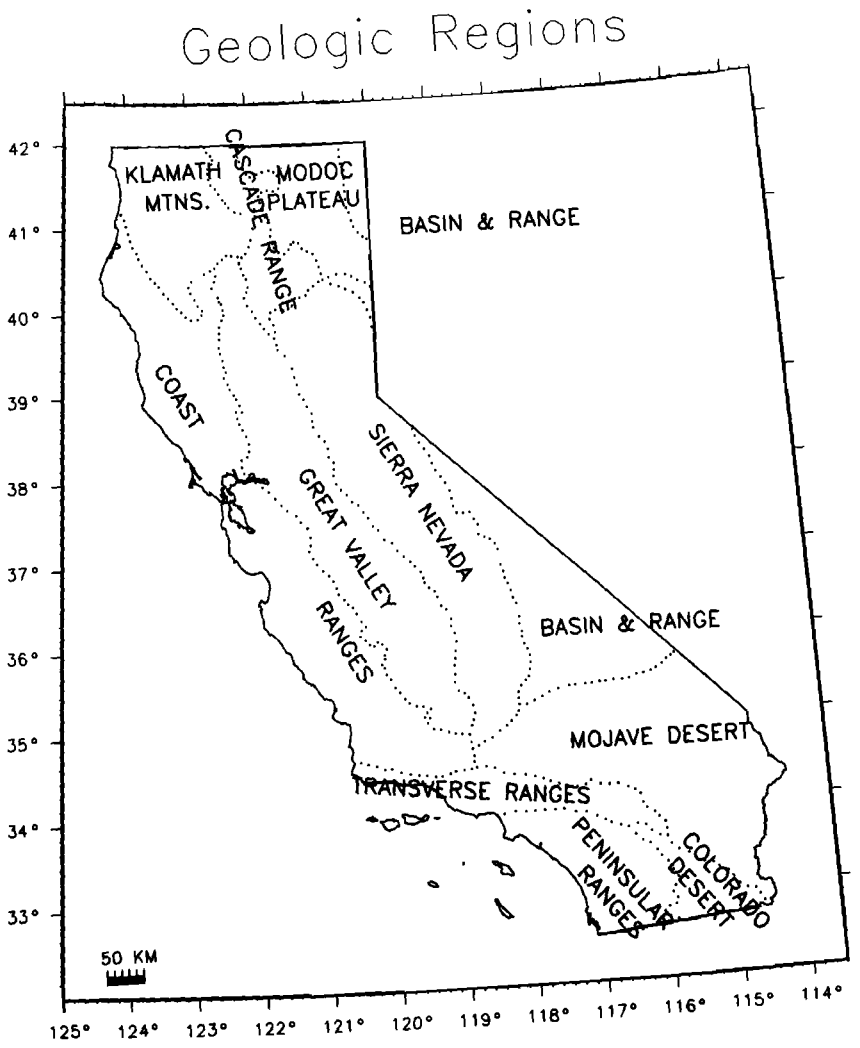

Fig. 12. Geologic regions of California (after 1938 map of O. P. Jenkins, as presented by *Hinds*, [1952].

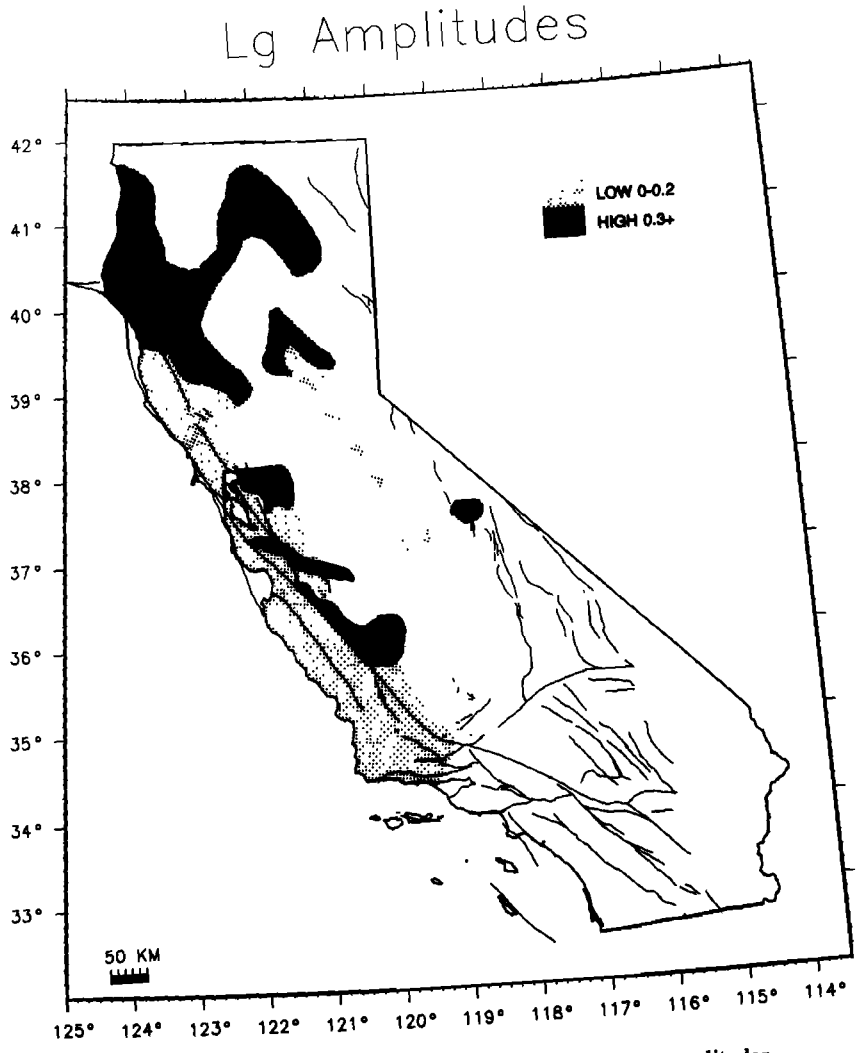

Fig. 13. Average *Lg* amplitudes in California. Average amplitudes were determined by filtering a 150-s time window of the *Lg* wave train with a two-pass zero-phase Butterworth filter from 1 to 15 s. The unstippled areas are those with inadequate information to determine an average amplitude.

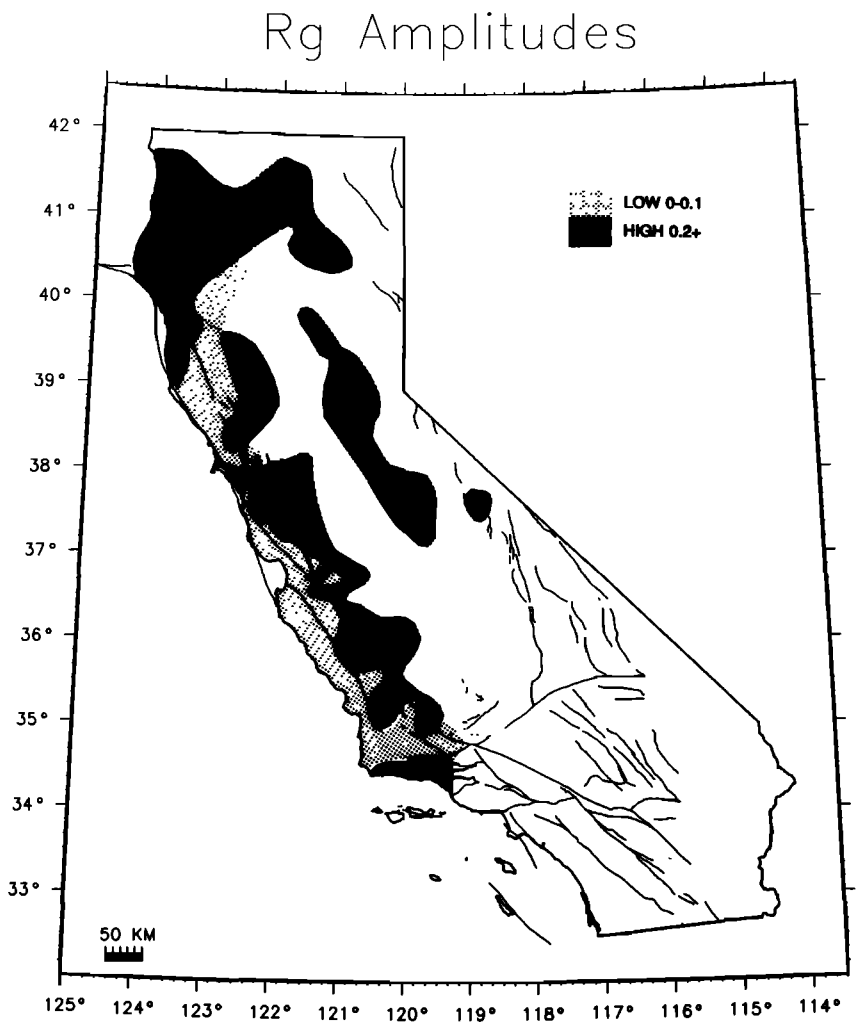

Fig. 14. Average *Rg* amplitudes in California. Average amplitudes were determined by filtering a 180-s time window of the *Lg* wave train with a two-pass zero-phase Butterworth filter from 5 to 15 s. The unstippled areas are those with inadequate information to determine an average amplitude.

Descriptions and groups of waveforms from each area can be found in the Appendix.

Discussion

Figure 15 is a comparison of the typical wave trains from each of the areas we discussed. An overall examination of the data reveals that the *Lg* and *Rg* waveform varies significantly throughout California, and the two types of surface waves are affected differently by crustal heterogeneities and changes in Moho depth. In general, *Lg* is more responsive to crustal features than is *Rg*, which is to be expected since *Lg* has shorter wavelengths. This information is important when using both *Lg* and *Rg* to map crustal features.

Another general observation is the higher interstation coherence in the N-S profiles (parallel to propagation) than in the E-W profiles (perpendicular to propagation). *Mrazek et al.* [1980] and *Der et al.* [1984] noted this same phenomenon in their data. This indicates forward scattering of energy from crustal heterogeneities [*Der et al.*, 1984]. Der et al. were able to rule out lateral anisotropy in the geological structure under the array used in their study as the cause of this coherence pattern. However, using only one event, we were unable to do that for this study. In general, interstation incoherency of waveforms is associated with areas of complex lithology and crustal structure such as the Coast Ranges, particularly south of San Francisco, and in the northern Sierra Nevada.

The thick sediments in the Great Valley seem to have a dramatic influence on the surface waves. The waveforms are amplified on profile C-C'and on the Great Valley records (Figures 5 and A5). The stations on the east side of the valley have a slightly higher amplitude than the surrounding area, but those stations on the west side of the valley have significantly larger amplitudes. This may indicate that the degree of amplification is dependent on the depth of the sediments, since the sediments are much thicker on the west side of the valley. Alternatively, the greater amplification of *Lg* and *Rg* in the west may be a result of the greater distance travelled by the waves in the thick sediments in the basin. This problem cannot be resolved without the addition of data from sources located at a range of azimuths. The amplification effect of the basin, in general, is consistent with *Campillo's* [1987] results from modeling of *Lg* waves in a sedimentary basin. On the other hand, *Gregerson* [1984] found that the 8-10 km of sediments in the Norwegian-Danish basin has almost no effect on the *Lg* wave.

The most interesting phenomenon that we see on the profiles is the change in the *Lg* and *Rg* wave trains in the vicinity of the San Andreas fault. This effect is most ev-

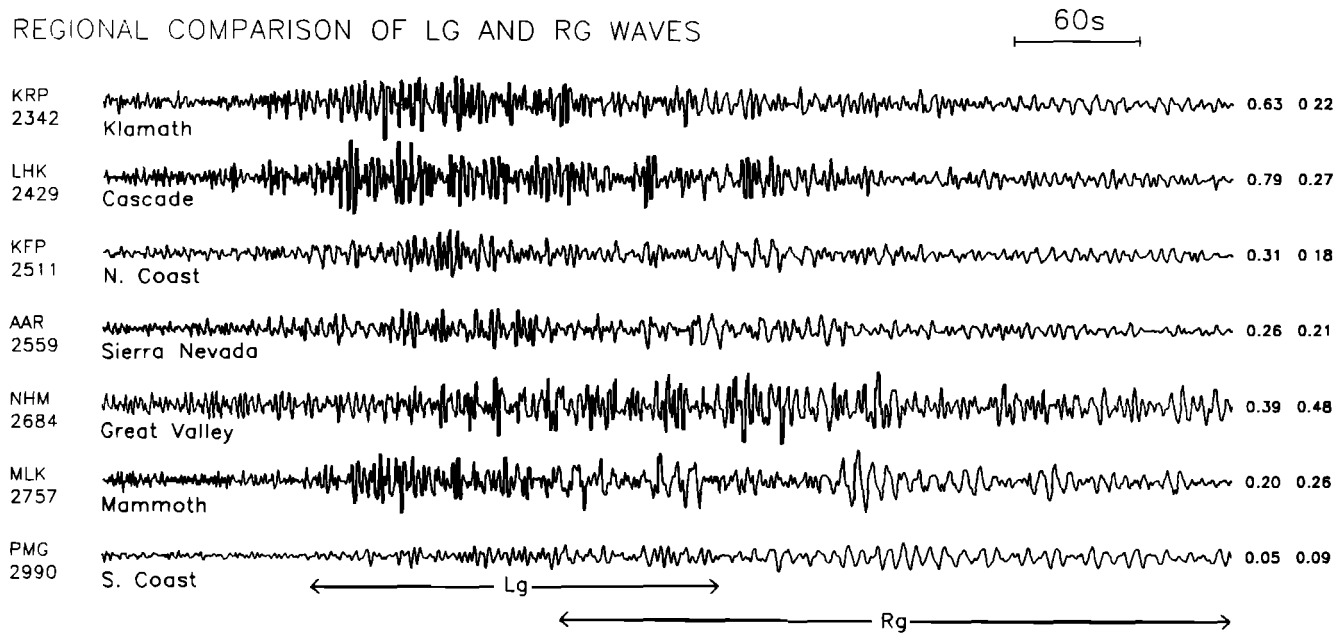

Fig. 15. Typical wave train from each geographical area studied. The epicentral distance of each station is shown below the station name. The average *Lg* and *Rg* amplitudes are shown to the right of each seismogram. The records are lined up by *Lg* arrival time, and the *Lg* and *Rg* wave trains are labeled.

ident on profiles B-B′ and E-E′ (Figures 4 and 7), but it appears on almost all profiles that cross the fault zone. The amplitudes of both *Lg* and *Rg* increase in the vicinity of the fault (although the increase is more pronounced in the *Lg* waves) and then decrease after crossing the fault zone. The short profiles across the fault zone parallel to the propagation direction (Figure 9), and the amplitude versus. distance plots associated with the profiles (Figures 10*a*-10*e*) further illustrate this phenomenon. The amplitude variation is convincing and leads us to conclude that the San Andreas fault (or the juxtaposition of different rock types on opposite sides of the fault) indeed alters the *Lg* and *Rg* waves.

Evidence of abrupt changes at the San Andreas fault include the following: *Zandt* [1981] showed that there is a linear low velocity zone subparallel to the San Andreas fault in the upper mantle. *Walter and Mooney* [1982] showed that the velocity structure and Moho depth on opposite sides of the San Andreas fault are different, with the Moho being shallower west of the fault. *Oppenheimer and Eaton* [1984] interpret the relatively early Pn residuals west of the San Andreas fault in their study as an indication of a lateral velocity contrast across the fault rather than a variation in crustal thickness. Nevertheless, their final results indicate that the Moho depth decreases gradually from about 39 km in the Sierra Nevada foothills to 22-24 km along the Pacific coast. The question of whether the abrupt change coincident with the San Andreas fault is a result of a change in the Moho depth or and change in rock types, or perhaps both, remains unresolved. However, we can compare our data with results of several theoretical studies involving *Lg* waves and changes in Moho depth. Let us consider both the possibility of a gradual decrease in the Moho and a sharp step in the Moho at the San Andreas fault.

If we assume that the Moho gradually decreases in depth toward the continent-ocean boundary, we have a model similar to *Kennett's* [1986] and *Regan and Harkrider's* [1989] transitional model. These two studies consider only *Lg* waves, and an important difference is that the waves in their models travel through the transition region normal to the structure. The waves travelling from the source in our study are arriving obliquely at the continent-ocean boundary. *Kennett* [1986] points out that obliquely travelling waves will show reduced effects of the boundary but may undergo other distortions since the waves spend a longer time in the transition zone. In any case, both *Kennett* [1986] and *Regan and Harkrider* [1989] predict that a thinning crust at a continent-ocean boundary will produce a concentrated waveguide and leakage of energy out of the bottom of the crust, particularly at higher frequencies. This should show up on a network of stations as an increased amplitude in the direction of the thinning crust due to the concentrated energy, followed by a decrease in amplitude from the continued leakage of energy into the mantle. The increase in amplitude of the *Lg* and *Rg* waves at the San Andreas fault occurs over a narrow area and is focused specifically at the fault, which leads us to presume that the amplification probably does not correspond to the concentration of energy that the two previously mentioned studies predict. The decrease in amplitude west of the fault may, however, correspond to a leakage of energy into the mantle due to the thinning crust.

Now if we assume that there is a sharp decrease in crustal thickness at the San Andreas fault, we have a model similar to *Regan and Harkrider's* [1989] step transition. This model predicts a sharp increase in amplitude approaching the step (a sharp decrease in crustal thickness) followed by a sharp decrease in amplitude. The increase in amplitude is due to energy reflected from the transition boundary. This model seems to fit our data better.

The average *Lg* amplitudes from north to south to California (Figure 11) seem to agree well with *Der et al.'s* [1984] predicted amplitude decay based on Δ^{-3}. The *Rg*

decay appears to be lower than the predicted theoretical 20-s Rayleigh wave decay of $\Delta^{-1.66}$ from the work of *Okal* [1989].

Characteristics associated with waveforms are consistent within particular regions. Regional patterns have been seen in other studies as well. *Gregersen* [1984] noticed a distinct regional pattern in *Lg* wave propagation near the North Sea and attributed it to path propagation differences. *Ruzaikin et al.* [1977] also saw regional *Lg* patterns in different parts of Asia. The areas exhibiting a large peak amplitude include a part of the Klamath Mountains and Cascade Mountains, the Great Valley, the Sierra Nevada, and a small area near the San Francisco Bay. Clearly, the large amplitude is due to more than one common factor among these areas. Amplification of seismic waves has been seen many times in sedimentary basins, so it is reasonable to assume that the thick layer of low-velocity sediments is the reason for the high amplitude in the Great Valley. The north Coast Ranges have low-amplitude or nonexistent *Rg* wave trains, while the south Coast Ranges have consistently low amplitude *Rg* wave trains.

The variation of group and phase velocity is also meaningful. We attempted to analyze the group velocity of both the *Lg* and the *Rg* waves, but the peak envelope was difficult to trace across the profiles and led to dubious results. Wave train length, the shape of the energy envelope, the frequency content, and the nature of the onset of the phases also reflect regional variations.

The north Coast Ranges have an *Lg* onset characterized by about 40 s of 0.15- to 0.2-Hz energy followed by the more typical *Lg* short-period energy for the duration of the wave train. This area also displays a gradual *Rg* onset if *Rg* is present at all. The south Coast Ranges, on the other hand, have a sharper *Lg* onset and more *Rg* content. The records from stations in the Cascade Range have a relatively sharp *Rg* onset. In the Sierra Nevada, *Lg* has a gradual onset and a short duration resulting in records dominated by a clear longer-period *Rg* wave train. These regional variations suggest that it may be possible to map the extent of different geological or structural areas based on the *Lg* and *Rg* waveform patterns.

CONCLUSIONS

The enormous amount of short-period data from the California regional networks can be used not only for earthquake locations and magnitudes but also for waveform studies. These short-period regional seismograms can be a valuable source of information with a variety of applications. We constructed profiles of *Lg* and *Rg* waveforms both parallel and perpendicular to the direction of propagation and observed groups of records from different regions in California. *Lg* and *Rg* phases react differently to various crustal changes and heterogeneities in California, and in general, *Lg* is more sensitive to the propagation path than *Rg*. Surface wave train characteristics including amplitudes, coda duration, shape of the energy envelope, frequency content, and sharpness of the phase initiation clearly vary with differing geological or structural areas. The amplitudes are low and the coherence poor in the Coast Ranges. Both *Lg* and *Rg* are amplified by travel through the Great Valley, and the Sierra Nevada foothills exhibit clear, dominant *Rg* waves in the record. The decreasing Moho depth near the Pacific coast may have an influence on the amplitudes of the *Lg* and *Rg* phases. The most interesting observation is that the San Andreas fault appears to correspond with amplified *Lg* and *Rg* codas in the vicinity of the fault one and decreased amplitudes after the fault zone is crossed.

APPENDIX

Zucca et al. [1986] described the Klamath Mountains in the northwest corner of California as an imbricated stack of oceanic rock layers as interpreted from the many thin layers with several low-velocity zones. The records from this region (Figure A1) have fairly high amplitude *Lg* waves (0.4 average) and moderate amplitude *Rg* waves (0.2 average). Neither *Lg* nor *Rg* has a sharp onset.

The Cascade Mountains form a suture between the Klamath Mountains to the west and the Modoc Plateau to the east *Zucca et al.*, 1986]. Zucca et al. describe the crust beneath the Cascade Range as similar to that beneath the Klamath Mountain but composed of thicker layers without any low velocity zones. The most noticeable characteristic of the wave trains in this region, seen in Figure A2, is their large amplitudes, particularly for *Lg* waves with an average of 0.8 units. The *Rg* amplitudes average about 0.3 units. The most interesting feature in this group of records is seen in the records from LHE and LMP, located on the north flank of Mount Shasta volcano. The *Lg* and *Rg* codas exhibit ringing and do not show any distinct arrivals. Station OSU, located on the north flank of the Sutter Buttes volcano in the Great Valley, also exhibits this same ringing. These three records do not provide sufficient data from which to draw a conclusion about the characteristics of *Lg* and *Rg* codas from stations located on the flanks of volcanoes, but the correlation between the volcanoes and the ringing is curious nonetheless.

The north Coast Ranges span the northern California coastline, including the Franciscan rocks of the Coastal belt, Central belt, and the Yolla Bolly belt [*Blake and Jones*, 1981]. The stations chosen for this group (shown in Figure A3) exhibit about 40 s of longer-period energy (0.15-0.2 Hz) at the initiation of the *Lg* wave on all but KCR and KKP at the north end of the group of stations. These two stations are the two farthest inland in this selected group. The *Lg* amplitudes are moderate with an average of 0.3 units, and the same is true for the *Rg* waves with an average amplitude of 0.1 units. The five northernmost stations, however, have higher than average *Lg* amplitudes for this region. The high-frequency *Lg* energy groups are not coherent from record to record, but some of the longer-period *Rg* energy shows coherence between records.

The south Coast Ranges span the southern California coastline from the Monterey Bay area south to the Transverse Ranges. They are composed of the plutonic and metamorphic rocks of the Salinian block, bordered on the SW by the Sur-Nacimiento fault zone and the Franciscan assemblage, and on the NE by the San Andreas fault and, once again, the Franciscan rocks. The group of stations shown in Figure A4 extends from the Monterey Bay area to just north of the Transverse Ranges. The *Lg* waveforms are particularly varied in amplitude, yet there are a few coherent energy group arrivals on some of the records. The amplitudes appear to be higher for stations located on the granitic Salinian block than those located on the Franciscan terrane, although there are exceptions. Station PMG, for example, has a low amplitude, yet it is underlain by the Salinian

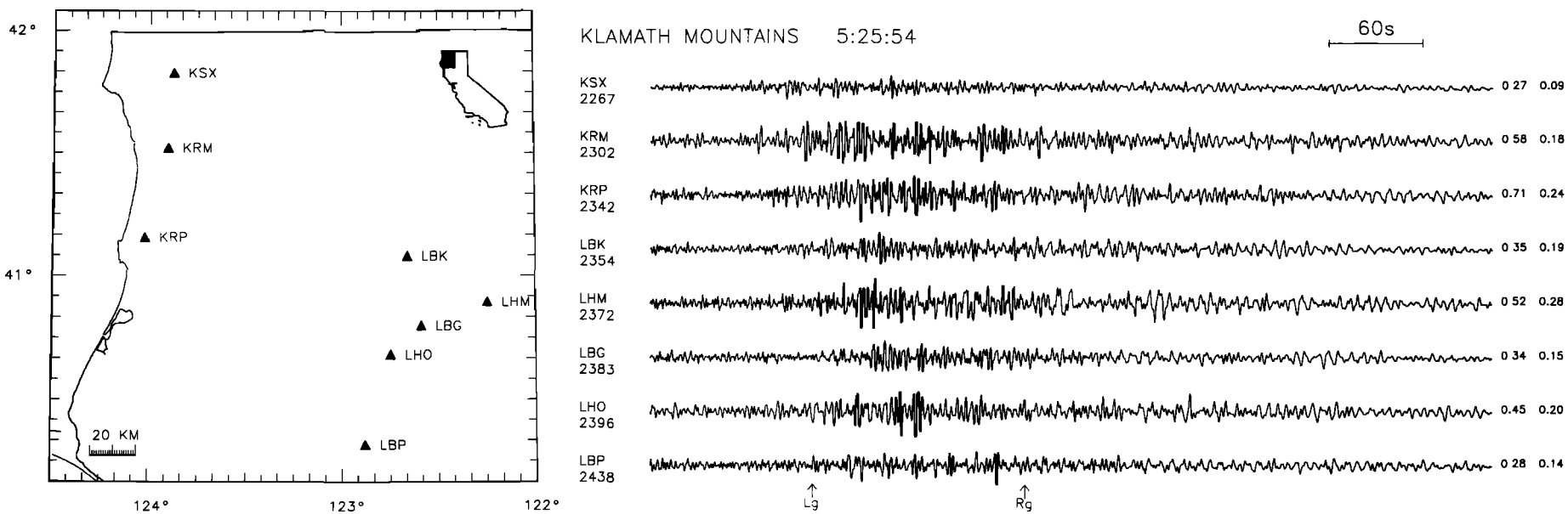

Fig. A1. Records from the Klamath Mountains. Approximate initiation of *Lg* and *Rg* is shown. The epicentral distance of each station is shown below the station name. The average *Lg* and *Rg* amplitudes are shown to the right of each seismogram.

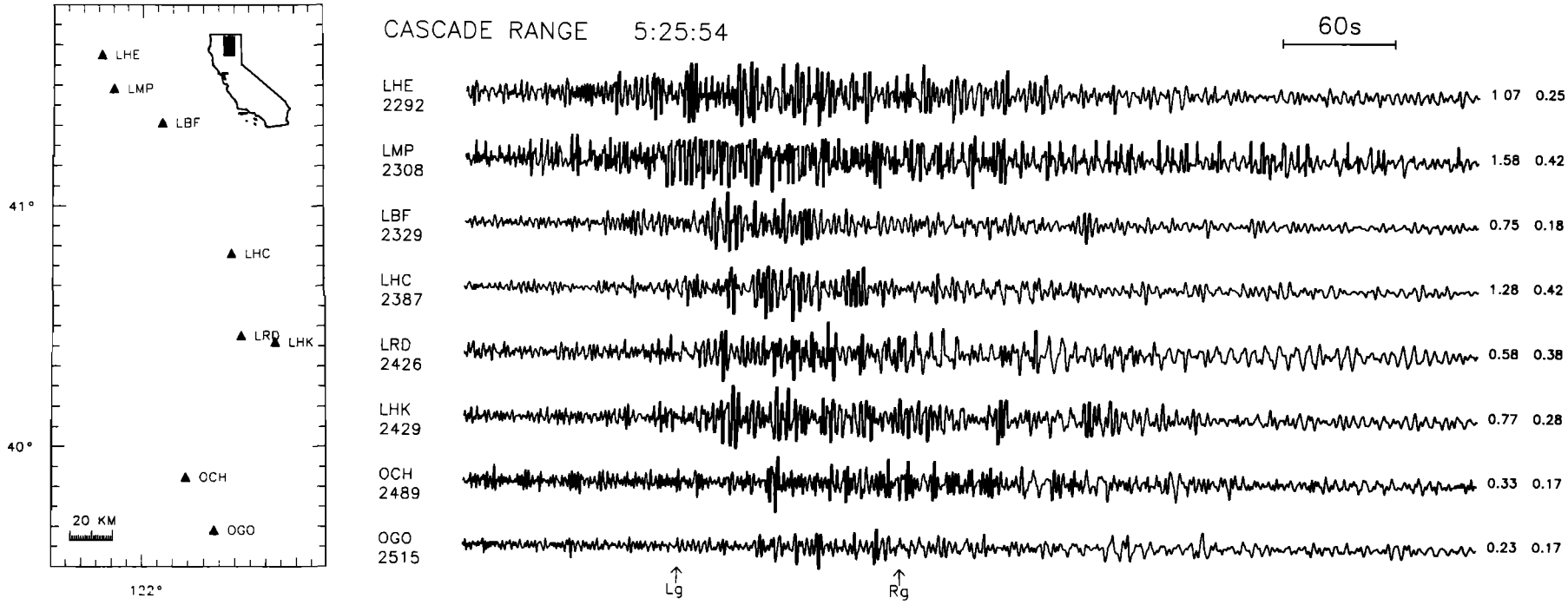

Fig. A2. Records from the Cascade Range. Approximate initiation of *Lg* and *Rg* is shown. The epicentral distance of each station is shown below the station name. The average *Lg* and *Rg* amplitudes are shown to the right of each seismogram.

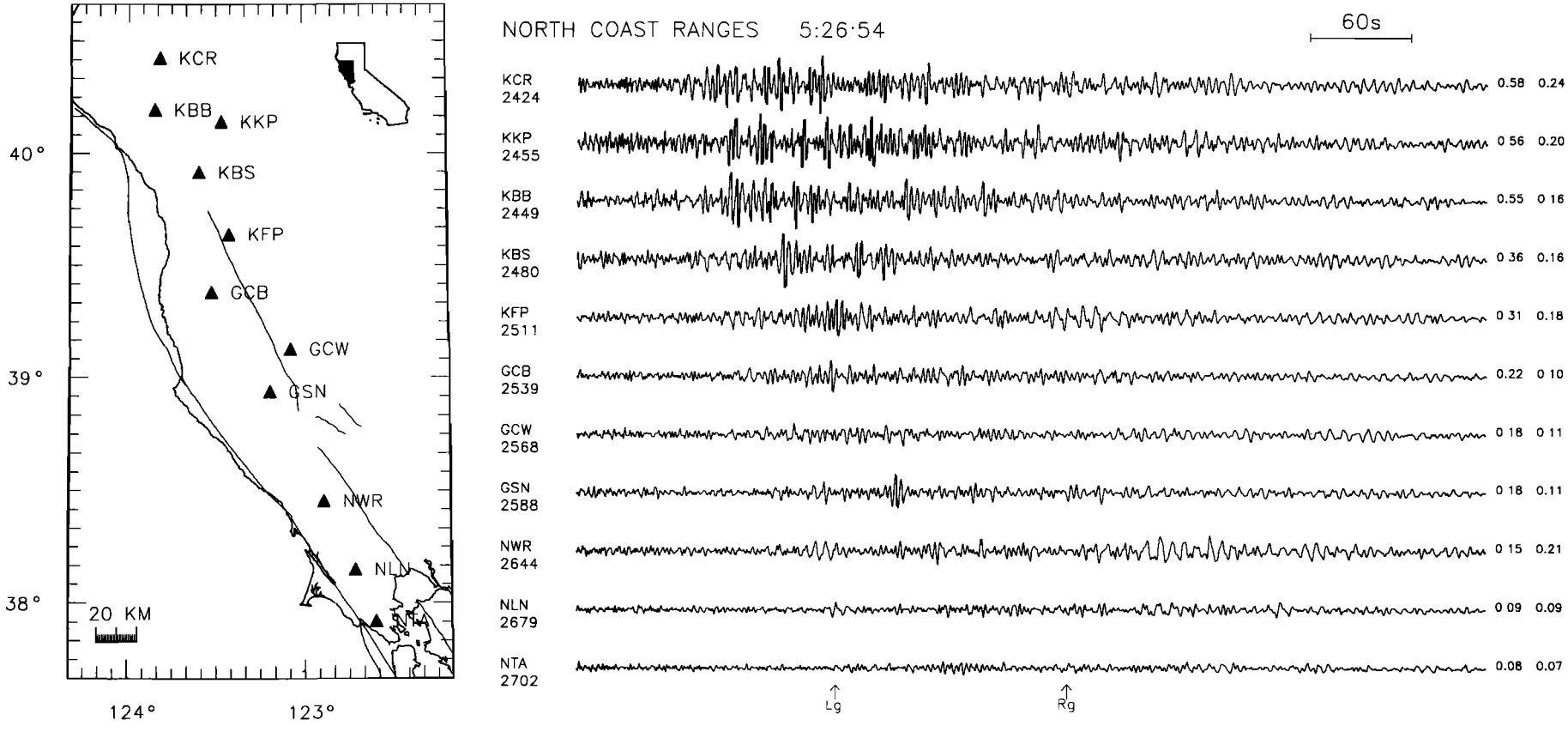

Fig. A3. Records from the north Coast Ranges. Approximate initiation of *Lg* and *Rg* is shown. The epicentral distance of each station is shown below the station name. The average *Lg* and *Rg* amplitudes are shown to the right of each seismogram.

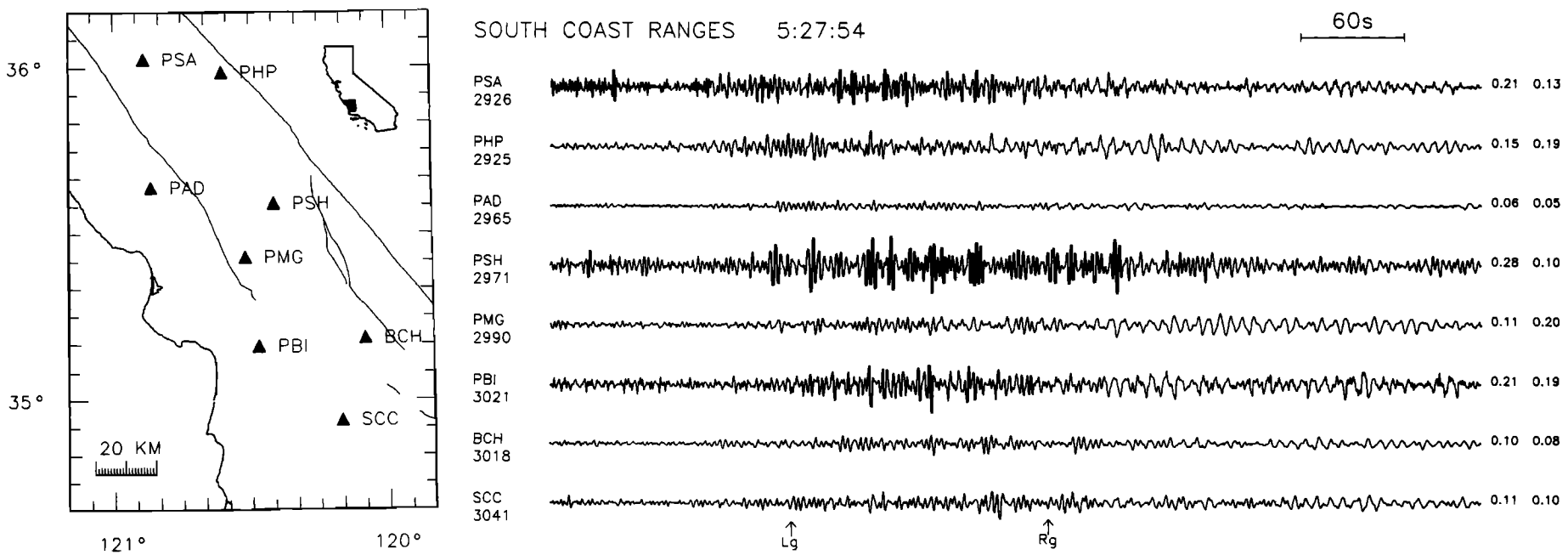

Fig. A4. Records from the south Coast Ranges. Approximate initiation of *Lg* and *Rg* is shown. The epicentral distance of each station is shown below the station name. The average *Lg* and *Rg* amplitudes are shown to the right of each seismogram.

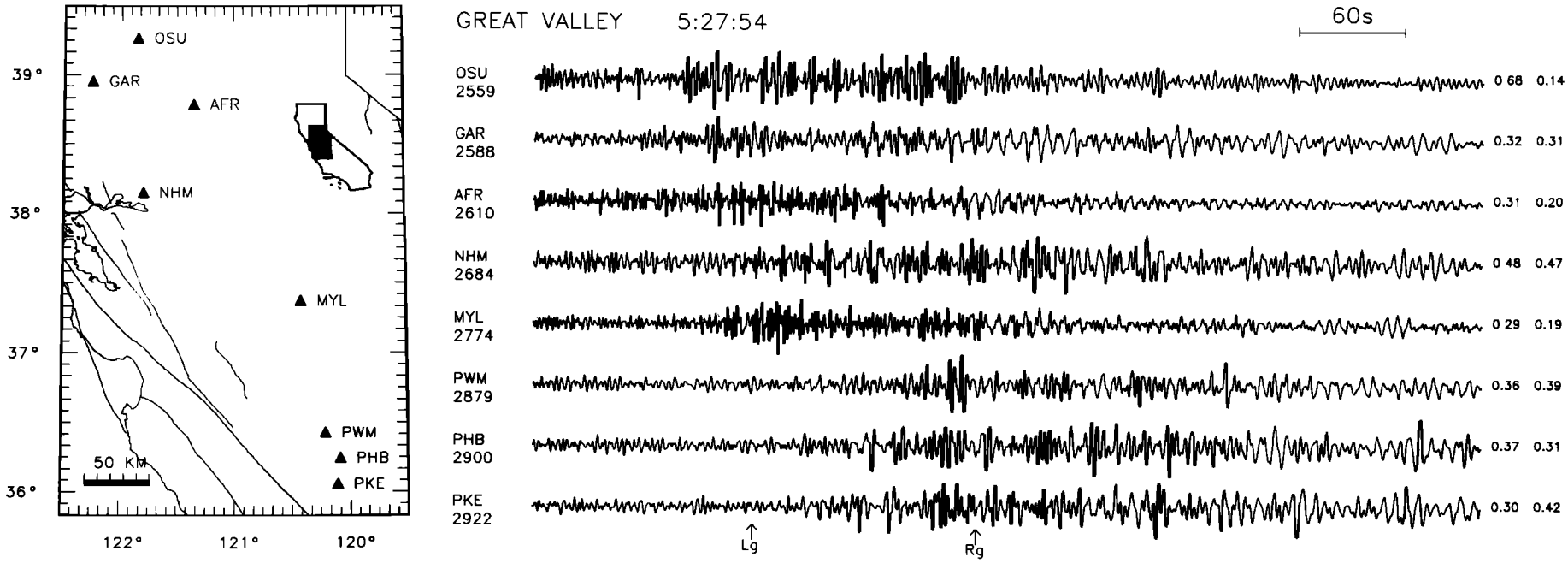

Fig. A5. Records from the Great Valley. Approximate initiation of *Lg* and *Rg* is shown. The epicentral distance of each station is shown below the station name. The average *Lg* and *Rg* amplitudes are shown to the right of each seismogram.

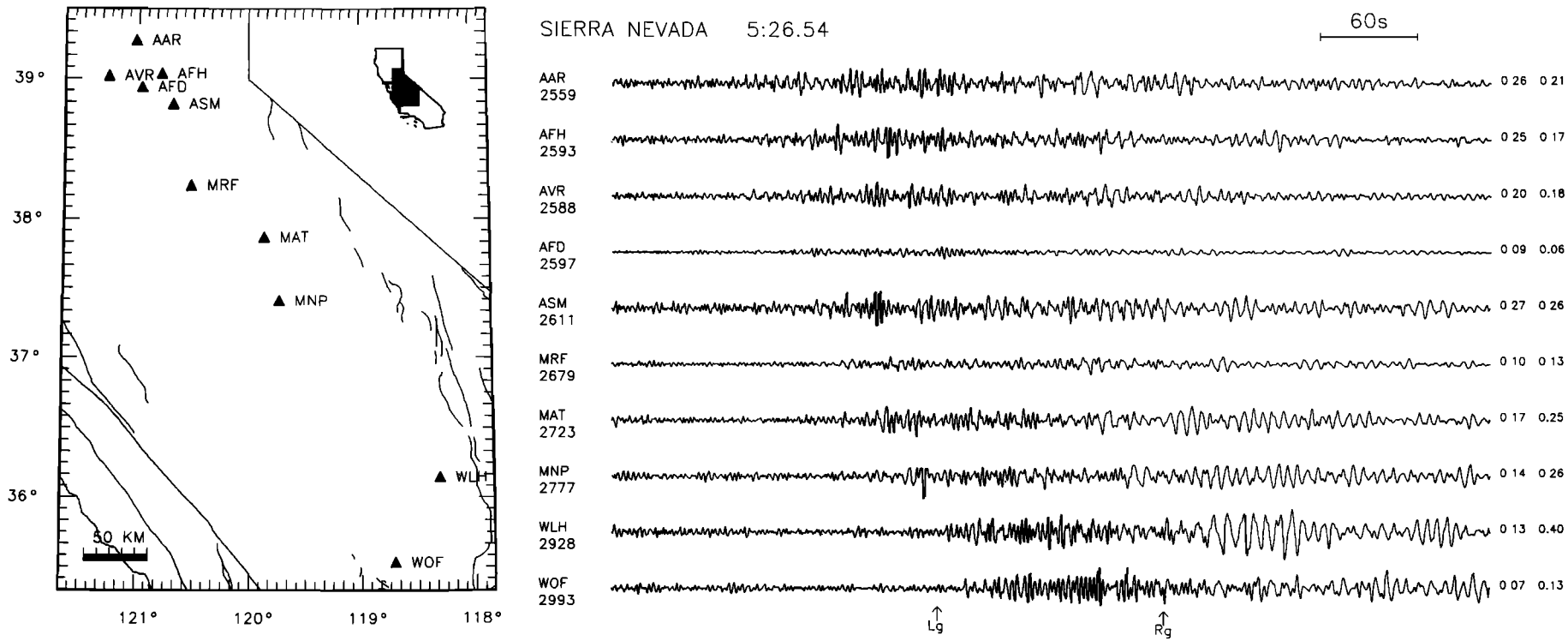

Fig. A6. Records from the Sierra Nevada. Approximate initiation of *Lg* and *Rg* is shown. The epicentral distance of each station is shown below the station name. The average *Lg* and *Rg* amplitudes are shown to the right of each seismogram.

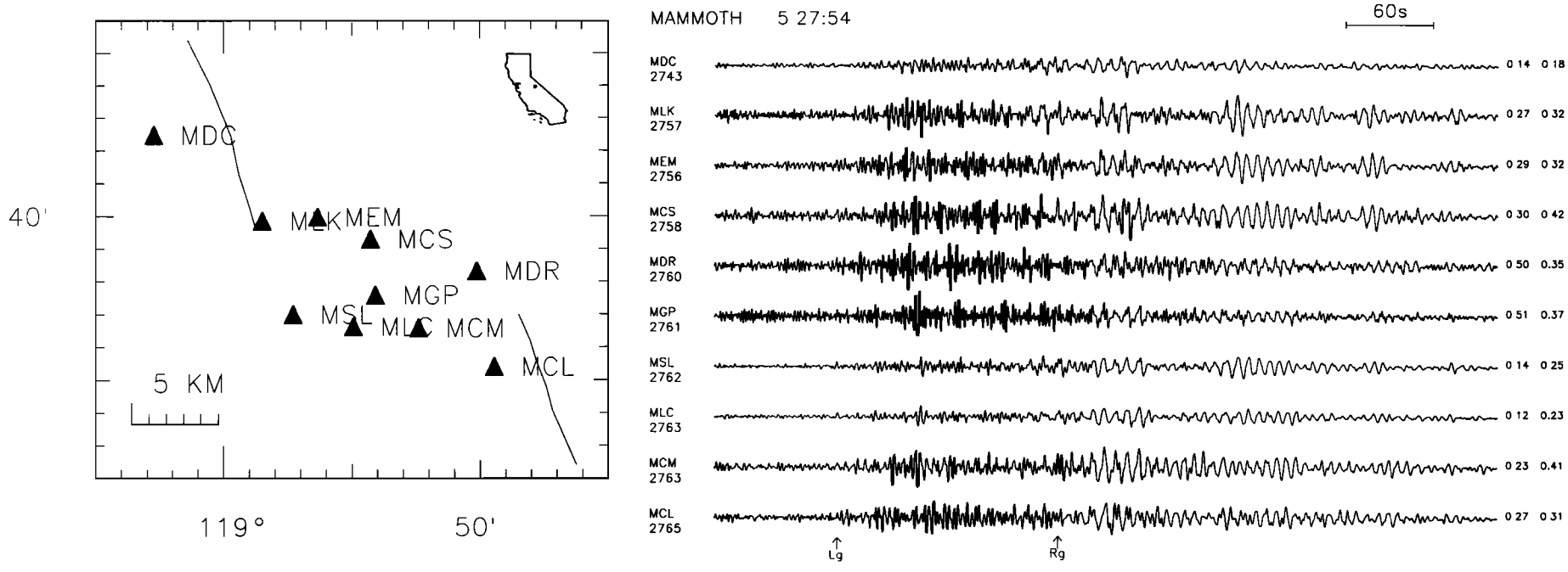

Fig. A7. Records from the Mammoth area. Approximate initiation of *Lg* and *Rg* is shown. The epicentral distance of each station is shown below the station name. The average *Lg* and *Rg* amplitudes are shown to the right of each seismogram.

block, and PBI has a high amplitude and is located on the Franciscan assemblage. Unlike the north Coast Ranges, *Rg* appears to have a more consistent average amplitude of 0.2 units and, in general, the same characteristic wave train.

The Great Valley of central California is a northwest trending asymmetric basin (deepest in the west) 700-km-long and 100-km-wide filled with as much as 6-9 km of sediment overlying a crystalline basement [*Hwang and Mooney*, 1986; *Colburn and Mooney*, 1986]. Unfortunately, very few stations are located in the valley. Most of the stations in this group are located around the perimeter of the valley, with the exception of OSU on the flank of Sutter Buttes volcano in the center of the northern valley (see Figure A5). Station OSU, in fact, produced a record distinct from all the others with a long duration of high-frequency ringing and a low *Rg* amplitude. This record looks much like the records from stations LHE and LMP (Figure A2), also located on the flank of the Mount Shasta volcano.

The valley sediments have a dramatic effect on the amplitude of the surface waves travelling through it, producing some of the largest surface waves (next to those in the Cascades) observed in this study. The *Rg* amplitude averages 0.3 units and the *Lg* averages 0.3 units. The three southernmost stations have the longest travel path through the valley and, correspondingly, the highest amplitudes.

The Sierra Nevada batholith trends parallel to the Great Valley. The Moho dips steeply from 27 km under the Great Valley to a depth of about 40 km under the Sierra Nevada [*Eaton*, 1963; *Prodehl*, 1979; *Mavko and Thompson*, 1983; *Oppenheimer and Eaton*, 1984]. The western foothills of the range are metamorphic, and this is where most of the stations in this study are located. Figure A6 shows that the *Lg* and *Rg* energy is coherent between stations in this area, and the amplitude tends to increase to the south, although there is much variation from station to station. The duration of the high-amplitude *Lg* wave train is relatively short compared to the duration in other areas, and the records are largely dominated by the *Rg* wave train. Most of the stations in the north are located in a complex geologic zone with a network of north-south and northwest-southeast trending faults. The amplitudes in this area of the Sierra Nevada are moderate.

The densest group of stations in this study is in the Mammoth area shown in Figure A7. Even though the waveforms from these stations are very coherent (due to the closely spaced stations), the amplitudes vary considerably over short distances. The *Rg* amplitudes differ by as much as a factor of 2, but the *Lg* amplitudes differ by as much as a factor of 4. The amplitudes seem to gradually increase to the south, and then there is a sharp drop-off in the amplitudes within a 3-km distance. Both the *Lg* and *Rg* arrivals are distinct on the record, and the *Rg* wave train is more consistently dominant on these records than in any other area.

Acknowledgments. We would like to acknowledge Bob Somera at the USGS in Menlo Park for digitizing the FM analog tape and Jerry Eaton, also in Menlo Park, for providing gain information for the Central California Network stations. We would also like to thank Toshiro Tanimoto and Dave Harkrider of Caltech for providing helpful comments and suggestions. David Hill, Rufus Catchings, David Wald, and two anonymous reviewers provided reviews which greatly improved this document.

References

Båth, M., The elastic waves *Lg* and *Rg* along Euroasiatic paths, *Ark. Geofys., 2*, 295–324, 1954.

Bateman, P. C., Geologic and geophysical constraints on models for the origin of the Sierra Nevada bathlith, California, in *The Geotectonic Development of California, Rubey Vol. I*, edited by W. G. Ernst, pp. 71–86, Prentice-Hall, Englewood Cliffs, N.J., 1981.

Blake, M. C., Jr., and D. L. Jones, The Fransiscan assemblage and related rocks in northern California: A reinterpretation, in *The Geotectonic Development of California, Rubey Vol. I*, edited by W. G. Ernst, pp. 306–328, Prentice-Hall, Englewood Cliffs, N.J., 1981.

Bouchon, M., The complete synthesis of seismic crustal phases at regional distances, *J. Geophys. Res., 87*, 1735–1741, 1982.

Campillo, M., Sismogrammes synthetiques dans les milieux elastiques heterogenes, developpement methodologique et applications, Thesis of Doctorat es Sciences Physiques (in French), Univ. of Grenoble, Grenoble, France, 1986.

Campillo, M., *Lg* wave propagation in a laterally varying crust and the distribution of the apparent quality factor in central France, *J. Geophys. Res., 92*, 12,604–12,612, 1987.

Campillo, M., J. L. Plantet, and M. Bouchon, Frequency dependent attenuation in the crust beneath central France from *Lg* waves: data analysis and numerical modeling, *Bull. Seismol. Soc. Am., 75*, 1395–1411, 1985.

Cara, M., and J. B. Minster, Multi-mode analysis of Rayleigh-type *Lg*. Part 1. Theory and applicability of the method, *Bull. Seismol. Soc. Am., 71*, 973–984, 1981.

Cara, M., J. B. Minster, and R. LeBras, Multi-mode analysis of Rayleigh-type *Lg*. Part 2. Application to southern California and the northwestern Sierra Nevada, *Bull. Seismol. Soc. Am., 71*, 985–1002, 1981.

Colburn, R. H., and W. D. Mooney, Two-dimensional velocity structure along the synclinal axis of the Great Valley, California, *Bull. Seismol. Soc. Am., 76*, 1305–1322, 1986.

Der, Z. A., A. O'Donnell, and P. J. Klouda, An investigation of attenuation, scattering and site effects on regional phases, Rep. VSC-TR-81-11, Teledyne Geotech, Alexandria, Va., 1981.

Der, Z. A., M. E. Marshall, A. O'Donnell, and T. W. McElfresh, Spatial coherence structure and attenuation of the *Lg* phase, site effects, and the interpretation of the *Lg* coda, *Bull. Seismol. Soc. Am., 74*, 1125–1147, 1984.

Eaton, J. P., Crustal structure from San Fransisco, California, to Eureka, Nevada, from seismic-refraction measurements, *J. Geophys. Res., 68*, 5789–5806, 1963.

Given, D. D., L. K. Hutton, and L. M. Jones, The Southern California Network Bulletin, July-December, 1986, *U.S. Geol. Surv. Open File Rep. 87–488*, 1987.

Gregersen, S., *Lg*-wave propagation and crustal structure differences near Denmark and the North Sea, *Geophys. J. R. Astron. Soc., 79*, 217–234, 1984.

Herrmann, R. B. and A. Kijko, Modeling some empirical *Lg* relations, *Bull. Seismol. Soc. Am., 73*, 157–171, 1983.

Hinds, N. E. A., Evolution of the California Landscape, *Bull. Calif. Div. Mines Geol., 158*, 1952.

Hwang, L. J., and W. D. Mooney, Velocity and Q structure of the Great Valley, California, based on synthetic seismogram modeling of seismic refraction data, *Bull. Seismol. Soc. Am., 76*, 1053–1067, 1986.

Johnson, C. E., CUSP - Automated processing and management for large regional networks, *Eos Trans. AGU, 62*, 957, 1983.

Kafka, A. L., and E. C. Reiter, Dispersion of *Rg* waves in southeastern Maine: evidence for lateral anisotropy in the shallow crust, *Bull. Seismol. Soc. Am., 77*, 925–941, 1987.

Kennett, B. L. N., On regional S, *Bull. Seismol. Soc. Am., 75*, 1077–1086, 1985.

Kennett, B. L. N., *Lg* waves and structural boundaries, *Bull. Seismol. Soc. Am., 76*, 1133–1141, 1986.

Knopoff, L., F. Schwab, and E. Kausel, Interpretation of *Lg*, *Geophys. J. R. Astron. Soc.*, *33*, 389–404, 1973.

Levshin, A. L., *Surface and Channel Seismic Waves*, (in Russian), Nauka, Moscow, 1973.

Mavko, B. B., and G. A. Thompson, Crustal and upper mantle structure of the northern and central Sierra Nevada, *J. Geophys. Res.*, *88*, 5874–5892, 1983.

Mooney, W. D., and R. H. Colburn, A seismic-refraction profile across the San Andreas, Sargent, and Calaveras faults, west-central California, *Bull. Seismol. Soc. Am.*, *75*, 175–191, 1985.

Mrazek, C. P., Z. A. Der, B. W. Barker, and A. O'Donnell, Seismic array design for regional phases, in Studies of Seismic Wave Characteristics at Regional Distances, Rep. AL-80-1, Teledyne Geotech, Alexandria, Va., 1980.

North, R. G., Instrumental distortion of m_bLg magnitudes, *Eos Trans. AGU*, *66*, 953–954, 1985.

Nuttli, O. W., Seismic wave attenuation and magnitude relations for eastern North America, *J. Geophys. Res.*, *78*, 5212–5218, 1973.

Nuttli, O. W., *Lg* magnitudes of selected east Kazakhstan underground explosions, *Bull. Seismol. Soc. Am.*, *76*, 1241–1251, 1986.

Okal, E. A., A theoretical discussion of time domain magnitudes: The Prague Formula for M_s and the mantle magnitude M_m, *J. Geophys. Res.*, *94*, 4194–4204, 1989.

Oppenheimer, D. H., and J. P. Eaton, Moho orientation beneath central California from regional earthquake travel times, *J. Geophys. Res.*, *89*, 10267–10282, 1984.

Page, B. M., The southern Coast Ranges, in *The Geotectonic Development of California, Rubey Vol. I*, edited by W. G. Ernst, pp. 329–417, Prentice-Hall, Englewood Cliffs, N.J., 1981.

Press, F., and M. Ewing, Two slow surface waves across North America, *Bull. Seismol. Soc. Am.*, *42*, 219–228, 1952.

Prodehl, C., Crustal structure of the western United States, *U.S. Geol. Surv. Prof. Pap.*, *1034*, 1979.

Regan, J., and D. G. Harkrider, Numerical modelling of SH *Lg* waves in and near continental margins, *Geophys. J. Int.*, *98*, 107–130, 1989.

Rivers, D. W., Effect of crustal structure on *Lg*, Rep. SDAC-TR-80-7b, Teledyne Geotech, Alexandria, Va., 1980.

Ruzaikin, A. I., I. L. Nersesov, and V. I. Khanturin, Propagation of *Lg* and lateral variations in crustal structure in Asia, *J. Geophys. Res.*, *82*, 307–316, 1977.

Shin, T. C. and R. B. Herrmann, *Lg* attenuation and source studies using 1982 Miramichi data, *Bull Seismol. Soc Am.*, *77*, 384–397, 1987.

Walter, A. W., and W. D. Mooney, Crustal structure of the Diablo and Gabilan Ranges, central California: a reinterpretation of existing data, *Bull. Seismol. Soc. Am.*, *72*, 1567–1590, 1982.

Wetmiller, R. J., R. B. Horner, H. S. Hasegawa, R. G. North, M. Lamontagne, D. H. Weichert, and S. G. Evans, An analysis of the 1985 Nahanni earthquakes, *Bull. Seismol. Soc. Am.*, *78*, 590–616, 1988.

Zandt, G., Seismic images of the deep structure of the San Andreas fault system, central Coast Ranges, California, *J. Geophys. Res.*, *86*, 5039–5052, 1981.

Zucca, J. J., G. S. Fuis, B. Milkereit, W. D. Mooney, and R. D. Catchings, Crustal structure of northeastern California, *J. Geophys. Res.*, *91*, 7359–7382, 1986.

T.H. Heaton and L. A. Wald, U.S. Geological Survey, 525 South Wilson Avenue, Pasadena, CA 91106.

(Received May 25, 1990;
revised March 11, 1991;
accepted March 22, 1991.)